ORNL/TM-2017/694

Demonstration of a Rapid HPLC-ICPMS Direct Coupling Technique Using IDMS—Project Report: Part I

Benjamin D. Roach
Cole R. Hexel
Joseph M. Giaquinto

October 2017

OAK RIDGE NATIONAL LABORATORY
MANAGED BY UT-BATTELLE FOR THE US DEPARTMENT OF ENERGY

ORNL/TM-2017/694

Chemical Sciences Division
Nuclear Analytical Chemical and Isotopics Laboratories

DEMONSTRATION OF A RAPID HPLC-ICPMS DIRECT COUPLING TECHNIQUE USING IDMS—PROJECT REPORT: PART I

Benjamin D. Roach
Cole R. Hexel
Joseph M. Giaquinto

Date Published: October 2017

Prepared by
OAK RIDGE NATIONAL LABORATORY
Oak Ridge, TN 37831-6283
managed by
UT-BATTELLE, LLC
for the
US DEPARTMENT OF ENERGY
under contract DE-AC05-00OR22725

CONTENTS

LIST OF FIGURE

LIST OF TABLES

ACRONYMS

CIMS chemical and isotopics mass spectrometry

DAPA diaminopropanoic acid

DGA diglycolic acid

DOE Department of Energy

HFIR High-Flux Isotope Reactor

HIBA α-hydroxyisobutyric acid

HPIC high pressure ion chromatography

HPLC high pressure liquid chromatography

IC ion chromatography

ICPMS inductively coupled plasma mass spectrometry

IDMS isotope dilution mass spectrometry

LOD limit of detection

LOQ limit of quantitation

MOX mixed oxide

NACIL Nuclear Analytical Chemistry and Isotopics Laboratory

ORNL Oak Ridge National Laboratory

PDCA pyridine dicarboxylic acid

REDC Radiological Engineering and Development Center

REE rare earth element

RSD relative standard deviation

SD standard deviation

EXECUTIVE SUMMARY

Staff members working in chemical separations and inductively coupled plasma mass spectrometry have developed a rapid separation-direct analysis scheme to determine both concentration and isotopics of a suite of elements down to the low picogram level. To reach the goal of rapid analysis of post-detonation nuclear materials, this first phase in method development has shown both the sensitivity and stability to achieve the precise, low-level analyses required. By coupling a high pressure ion chromatography system to an inductively coupled plasma mass spectrometer, researchers can achieve online analysis of the separated components of the sample directly. Using the Thermo Scientific™ Qtegra™ analysis software, the data has been processed automatically to yield precise isotopic composition and concentrations.

1. INTRODUCTION

1.1 SCOPE OF WORK

This Oak Ridge National Laboratory (ORNL) report documents fiscal years 2015–2016 research efforts by the Nuclear Analytical Chemistry and Isotopics Laboratory's (NACIL's) Chemical and Isotopics Mass Spectrometry (CIMS) ultra-trace nuclear forensics facility. The work was used to confirm the predefined experimental strategies and served as a proof of concept for the rapid measurement of isotopic and elemental concentrations in a multielement system. The work was divided into three stages: developing the chemistry, determining the stability/reproducibility of the developed chemistry, and determining the chosen methods' limits of detection and quantitation. Whereas the data presented here show the development of a successful method, it must be stated that these results are for an ideal system where the analyte concentrations were equivalent and no matrix was imposed.

This work was undertaken to complete the Demonstration of a Rapid HPLC-ICPMS Direct Coupling Technique Using IDMS Project T2 in ORNL's DTRA J9-NTFC/A FY 2015 solicitation "MIDAS 15–Technical and Analytical Support for the DTRA/J9 Nuclear Forensics Office." The description of this task is stated as follows:

> Demonstrate the effectiveness of a rapid measurement protocol which directly couples High Pressure Liquid Chromatography (HPLC) and Inductively Coupled Plasma Mass Spectrometry (ICPMS). This technique would allow for rapid online HPLC chemical separations with direct isotopic detection and isotope ratio measurements using mass spectrometry and, with the incorporation of IDMS, improve accuracy and precision of the analyses over standard elemental and isotopic assay techniques.

The main intentions during this research were to determine the feasibility of a single multieluent separation scheme that would enable the separation and analysis of as many of the predetermined analytes as possible. The analysis consisted of injecting a multielement standard onto a high pressure chromatography column, and, using various chemical eluents to perform elemental separation, direct analysis using ICPMS. ICPMS enables the analysis of isotopic masses and, together with elemental separation, is the ideal tool to measure nonnatural isotopes/isotopic ratios. Further development of the method was to ensure sufficient capability to achieve measurements of elemental and isotopic signatures at levels likely to be present in post-detonation material. [1]

1.2 FACILITIES AND CAPABILITIES

The majority of the method development work for this project was undertaken in the CIMS Laboratory (Building 1005 at ORNL; see Figure 1), where the expertise is primarily high-precision isotopics and elemental assays with emphasis on U and Pu measurements by thermal and plasma-based multicollector mass spectrometers. The preparation and separation chemistries required to perform high precision measurements, together with trace clean handling of samples in class 100 and 1000 clean rooms, makes this facility the prime choice to investigate the methodology intended for subnanogram determination of impurities detections.

The equipment employed in the method development is a Thermo Scientific™ Dionex™ ICS-5000+ high pressure ion chromatography (HPIC) system (Figure 2, left) coupled to a Thermo Scientific™ iCAP™ Q quadrupole ICPMS (Figure 2, right). The HPIC system is composed of an AS-AP autosampler, complete with sample dilution and fraction collection capabilities; a gradient mixing pump, capable of combining four different eluents in the same analysis; and a thermal compartment containing the injection loop and separation column, able to maintain temperatures 5–85°C for constant elution times and reproducibility.

The ICPMS is equipped with a wide-range sensitivity detector (parts per million to smaller than parts per trillion), a robust torch capable of withstanding the introduction of salts and organic matter from the HPIC eluents, a wide bore nebulizer that can nebulize solutions of higher density and organic content, and a specialized collision cell that reduces the signal-to-noise ratio for high-precision measurements of low-mass analytes. For method development and testing, the system is set up in a nonradioactive facility; however, both systems (ICS5000+ HPIC and iCAP Q ICPMS) are available at the Radiological Engineering and Development Center (REDC), which operates in conjunction with the High Flux Isotope Reactor (HFIR). The REDC, a Category II nuclear facility, has been the nation's main center of production, storage, and distribution of transuranium elements for the US Department of Energy's (DOE's) heavy-element research program since 1966.

Figure 1. Photos of the Chemical and Isotopics Mass Spectrometry (CIMS) facility.

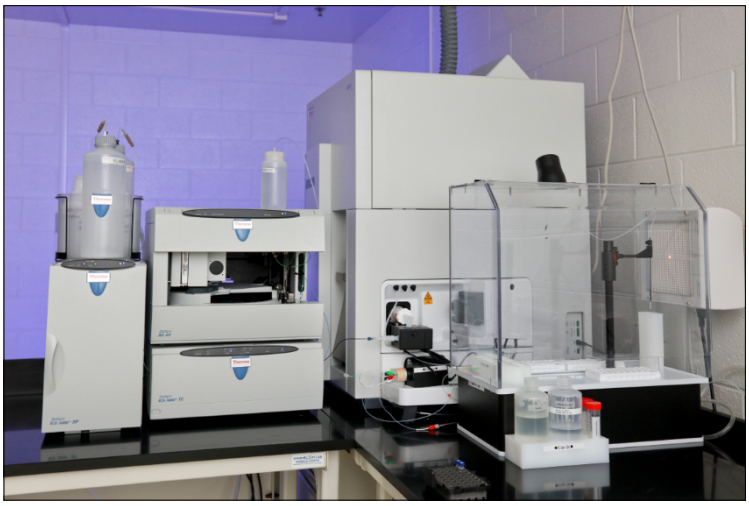

Figure 2. Photo of the current coupled high pressure ion chromatography (HPIC) and inductively coupled plasma mass spectrometry (ICPMS) system.

1.2.1 Previously Demonstrated Work

To illustrate previous success in the application of HPIC separations coupled with isotope dilution mass spectrometry (IDMS), some examples are described in the following sections.

1.2.1.1 Modeling the behavior of aluminum doped NpO_2 pellets

Researchers used ID-HPIC-ICPMS to provide empirical data to support modeling the behavior of aluminum doped NpO_2 pellets irradiated in HFIR for the production of Pu-238. High precision empirical data are required to validate sophisticated reactor depletion codes, especially given that the neutron cross sections for Np-239, one of the main fissile isotopes produced, are not very well known. The performance required for the analytical methods to provide meaningful data are to achieve relative standard deviations of 1–3% for the major fission-produced isotopes. This level of precision is critical to meaningful evaluations and uncertainty analyses of the depletion code performance. The HPLC-IDMS measurement protocol is providing ORNL depletion code experts with the empirical data that meets their demands. Analytical data for this project was recently completed. Figure 3 is an illustration of initial adjustments to the depletion models using the HPLC-IDMS fission product data for the high-mass rare earth elements (REE) as a guide. Uncertainties in the analytical data were calculated to be < 2% relative for the high mass REE atoms and ~ 8–10% relative for the low-mass atoms. Because this is a first pass, no uncertainties have been assigned to the model predictions. This illustration is shown only for a visual representation of the benefits of high precision measurements vs. conventional ICPMS measurements. It can be observed that the correlation of the measured vs. calculated low-mass atoms is not as tight as the same correlation for high-mass atoms.

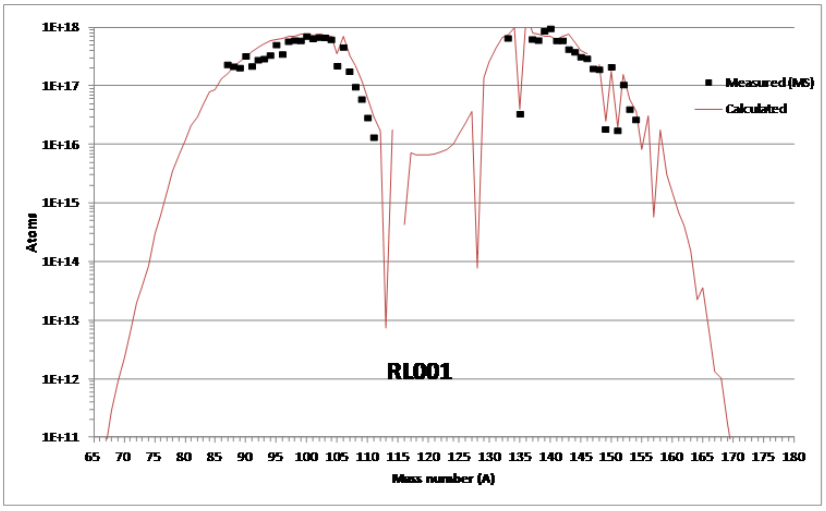

Figure 3. Calculated vs. measured for fission-produced atoms by mass number in an irradiated NpO_2 target. The low-mass atoms were calculated using standard inductively coupled plasma mass spectrometry calibrations, whereas the high-mass atoms were calculated using high pressure liquid chromatography and inductively coupled plasma mass spectrometry.

1.2.1.2 Improvements to commercial reactor depletion codes for mixed oxide fuels

The NACIL also used ID-HPIC for improvements to commercial reactor depletion codes for mixed oxide (MOX) fuels irradiated in US reactors. NACIL used this methodology to measure key rare earth and cesium fission products as well as uranium and plutonium in irradiated MOX fuels in support of the DOE Fissile Materials Disposition Program Office project to prove the feasibility of disposal of weapons grade

plutonium through use as a nuclear fuel.The data produced are being used to refine depletion models for fuel bundles to account for fuel rods at the periphery of the bundle and for those near the supports in the reactor core or water channels at which the neutron flux varies slightly compared with those in the center of the bundle. Figure 4 illustrates the accuracy and precision possible using HPLC-ICPMS when compared with a fuel rod in the center of the fuel bundle for which the neutronic code is well established. Shown is the axial burnup profile of the rod with three specimens analyzed for burnup. Measured burnup uncertainty was calculated to be ± 2.5% relative. Figure 5 illustrates a peripheral rod in the bundle for which the HPLC-ICPMS empirical data were used to demonstrate that more detailed neutronic calculations were required to predict depletion by fission. The dotted red line on the chart is a preliminary adjustment to the model using the HPLC-ICPMS empirical data generated for specimens 1 through 3. [2]

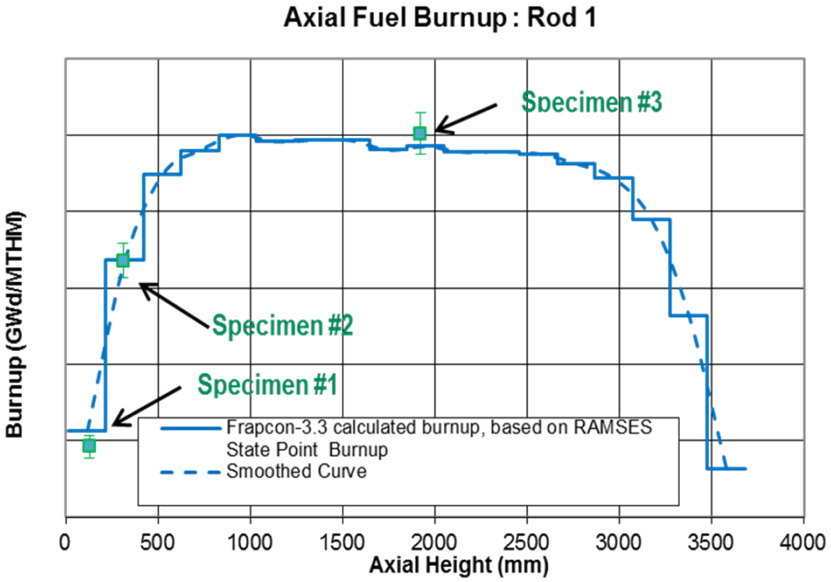

Figure 4. Illustration of the effectiveness of high pressure liquid chromatography and isotope dilution mass spectrometry (HPLC-IDMS) to provide high accuracy stable lanthanide data at the parts per million level in irradiated nuclear fuels. Nd-148 is a key burnup indicator and was measured using HPLC-IDMS as well as the fissional isotopes U-238, U-235, and Pu-239.

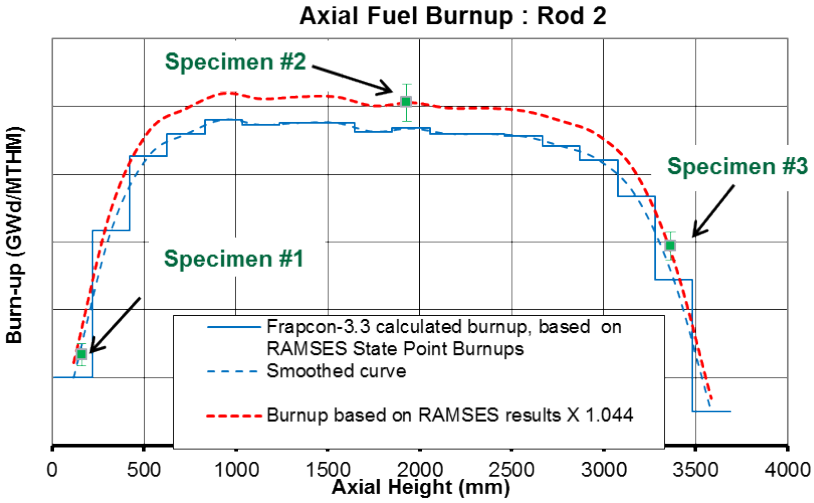

Figure 5. Peripheral rod for which more detailed neutronic calculations would be needed to better quantify the effects of neutronics on isotopics.

2. CHEMICAL SEPARATION TECHNIQUES

In HPIC, as with all ion-exchange chromatography, the analyte/analyte complexes are retained on the column based on ionic interactions with the stationary phase of the resin. The stationary phase of the ion chromatography (IC) column contains ionic functional groups (R-X) that interact with analyte ions/complexes of the opposite charge. There are two types of IC: cation exchange chromatography and anion exchange chromatography. The ionic compound consisting of the cationic species M+ and the anionic species B- can be retained by the stationary phase.

Cation exchange chromatography retains positively charged cations because the stationary phase displays a negatively charged functional group:

$$R\text{-}X^{-}C^{+} + M^{+}B^{-} \rightleftharpoons R\text{-}X^{-}B^{+} + C^{+} + B^{-}$$

Anion exchange chromatography retains anions using a positively charged functional group:

$$R\text{-}X^{+}A^{-} + M^{+}B^{-} \rightleftharpoons R\text{-}X^{+}B^{-} + M^{+} + A^{-}$$

In the method development of an effective separation, the ion strength of either C+ or A- in the eluent can be adjusted to shift the equilibrium position and, in turn, the retention time of the analytes. Cations can also be separated using anion chromatography as anionic complexes

The ion chromatograms below show separations of the rare earth elements effectuated using anion exchange (Figure 6) and cation exchange (Figure 7). These were performed using HPIC on an ICS-5000+ system employing a post-column chromophore and ultraviolet-visible spectroscopy detection according to protocols outlined by Dionex. [3, 4, 5]

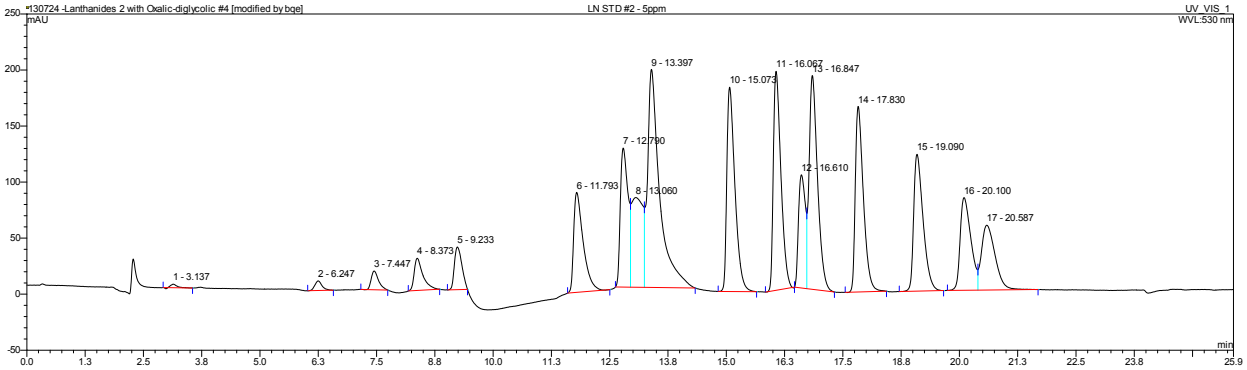

Figure 6. Anion exchange—using oxalic acid and diglycolic acid (buffered with LiOH) as the mobile phase and a sulfonic acid ion exchange resin. Lanthanides elute in order of decreasing ionic radius as anionic complexes.

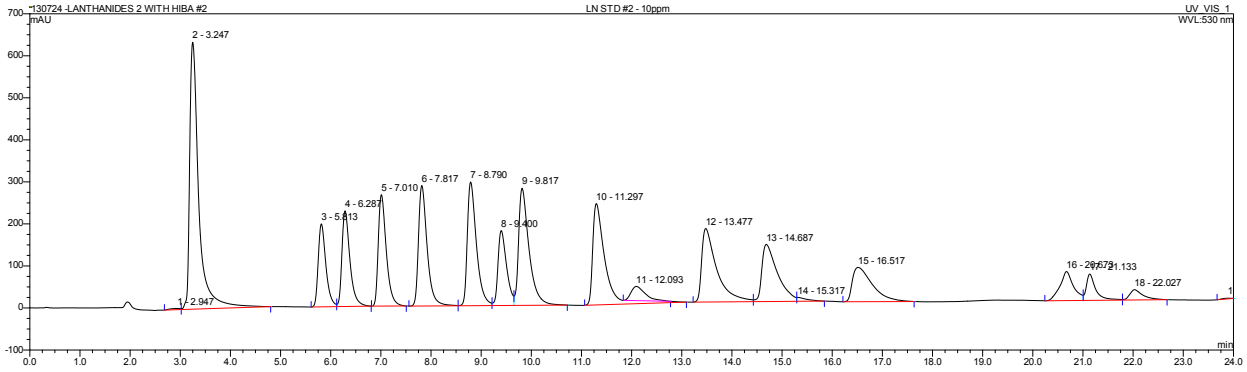

Figure 7. Cation exchange—using α-hydroxyisobutyric acid (buffered with LiOH) as the mobile phase and a tetra-alkylammonium ion exchange resin. Lanthanides elute in order of increasing ionic radius.

2.1 CHOICE OF HIGH PRESSURE ION CHROMATOGRAPHY (HPIC) COLUMN

2.1.1 Dionex CS10

The initial column to be chosen was the Dionex CS10 column, a sulfonic acid cation exchange resin with a high analyte loading capacity of 80 µequivalents/column. This column was chosen because of its successful application in the IDMS-HPIC separations to the doped NpO_2 pellets and mixed oxide spent fuel (see section 1.2.1.)

2.1.2 Dionex CS5A

The Dionex CS5A is a next-generation, dual-functionality column with mixed sulfonic acid cation exchange sites and tetra-alkylammonium anion exchange sites. Because of the dual functionality of this column, the loading capacity is lower than that of the CS10 column at 40 µequivalents/column. This column was chosen because of the potential sequential separation of both the transition metals and lanthanide elements within the same run using both the cation and anion exchange residues.

2.2 CHOICE OF ELUENTS

Because of the nature of the HPIC resins and the effect that greasy organic molecules and salts can have on the nebulization and ionization processes of the ICPMS, the choice of reagents was limited. Existing separation schemes published by Dionex were investigated for a number of factors, including the following:

- Separation of analytes
- Peak shape produced in the chromatogram
- Salt content and the effect on the ICPMS
- Organic concentration

2.2.1 Separation of Analytes

The primary factor for choosing an eluent is its ability to separate out the elemental analytes from one another before analysis. The main reason for this is to separate elements that contain isobaric interferences (isotopes of the same mass) to yield accurate elemental isotopics. It is also important to separate the analyte in question from any element that has the potential to form polyatomic interferences upon ionization that will result in an interference with a mass the same as the analyte in question. For example, cerium readily forms oxides in ICPMS, and the oxide of Ce-140 has a mass-to-charge ratio

(m/z) of 156, which would interfere with Dy-156 and Gd-156 if cerium wasn't separated from gadolinium and dysprosium.

2.2.2 Peak Shape

The shape of the peak isn't as vital to the analysis as the separation of analytes; the shape does, however, have an effect on the accuracy of the isotopic analysis and the detection limit of the method. A wide or elongated peak will have a higher signal-to-noise ratio, as will an uneven peak with a trailing baseline. The ideal peak would be symmetrical and would elute over as short a time as possible.

2.2.3 Salt/Organic Content

In ICPMS analyses, matrixes can have a serious effect on the sensitivity, reproducibility, and stability of a measurement. High salt content can result in the failure or clogging of the nebulizer as well as the potential to damage the lenses and ion optics. Although the option is available to employ an oxygen bleed into the plasma to help reduce any impact organic molecules may have on the system, the formation of oxides, however, may also affect the sensitivity of the analysis.

2.3 DEVELOPING ELUENT COMPOSITION FOR ICPMS STABILITY

The pH and ionic strength of the mobile phase are crucial for successful resin separations in ion chromatography. The pH of the mobile phase significantly affects the retention time of analytes. Changing the eluent pH may alter the extent to which the analytes are ionized, affecting the extent to which they interact with the stationary phase and, hence, their retention time. These changes in pH will lead to changes in retention time for the analytes, which may in turn lead to selectivity changes within the chromatogram. The ionic strength (salt content) of the chromatogram also can influence the retention times and selectivity of the analytes because it can alter the solubility of the resulting complex in the mobile phase.

Most commercially available mobile phases are buffered to a pH of 4–5 using a lithium or sodium hydroxide, which can have a significant effect on the stability of the mass spectrometer over extended periods. This salt-based buffering prevents the use of commercially available reagents and reagent formulations. In past work within the NACIL group, researchers have successfully buffered the eluent using ammonium hydroxide in the place of lithium hydroxide for an α-hydroxyisobutyric acid (HIBA) eluent used for the sequential elution of trace lanthanides from bulk uranium samples.

3. RESULTS

3.1 INITIAL EXPERIMENTS

3.1.1 HIBA Method

To determine the coupled system's efficacy in separating and detecting metals, researchers used an initial test that has been tried and tested by the NACIL group using an offline IC system with fraction collection capabilities. The analysis was performed according to a recent ASTM test method developed at ORNL for the separation of lanthanides from a bulk uranium matrix using HIBA and a CS-10 Dionex HPIC column (with sulfonic acid functional groups) in a cation exchange system (Figure 8).

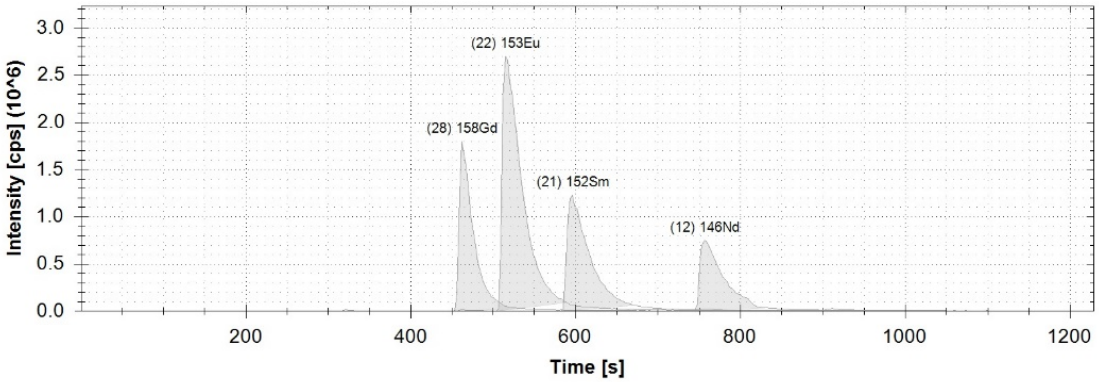

Figure 8. Cation exchange—using α-hydroxyisobutyric acid (buffered with NH_4OH) as the mobile phase and a tetra-alkylammonium ion exchange resin. Lanthanides elute in order of increasing ionic radius and are measured as the chosen isotopic mass in the chromatogram.

The separation of the lanthanides from the bulk uranium matrix is efficient, as is the sequential elution of the lanthanide analytes. The peak shape isn't ideal; however, proof of concept was achieved, and the observed ratios are shown to be within a few percent of known (Table 1).

Table 1. Observed ratios vs. natural ratios and the percent recovery of the chosen analytes, separated using the α-hydroxyisobutyric acid method

Element	Ratio	Natural ratio	Observed ratio	Percent recovery
Gadolinium	158/160	1.14	1.12	98%
Europium	151/153	0.92	0.91	99%
Samarium	149/152	0.52	0.51	98%
Neodymium	143/146	0.71	0.68	96%

3.1.2 Oxalic Acid and Diaminopropanoic Acid

Because the HIBA system proved to be successful, an anionic separation was also tested. Oxalic acid (0.1 M, buffered to pH 4.5 using ammonium hydroxide) was used in conjunction with diaminopropanoic acid (DAPA, 0.1 M, buffered to pH 4.5 using ammonium hydroxide) and the multifunctional CS-5A Dionex resin. Figure 9 illustrates the resulting chromatogram showing highly symmetrical peak shapes and quantitative separation. Table 2 details the gradient elution using oxalic acid, diaminopropanoic acid,

and deionized water to adjust the concentrations. As with the HIBA method, the isotopic ratios of the analyte lanthanides were within a few percent of known as shown in Table 3.

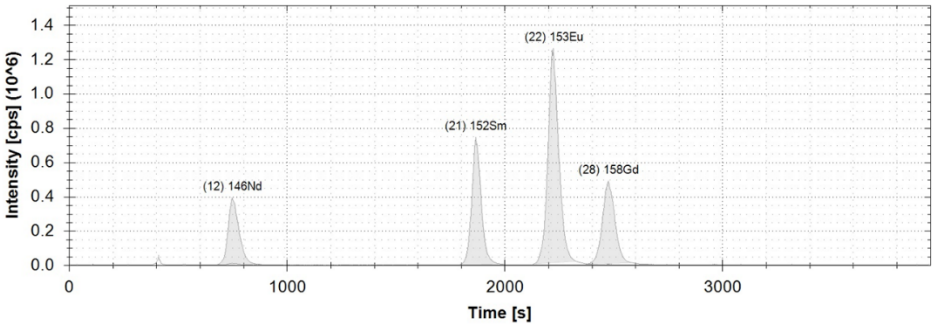

Figure 9. Anion exchange—using a mixed oxalic acid and diaminopropanoic acid gradient elution (buffered with NH_4OH) as the mobile phase. Lanthanides elute in order of decreasing ionic radius and are measured as the chosen isotopic mass in the chromatogram.

Table 2. Gradient elution profile for an oxalic acid and diaminopropanoic acid separation used to produce the chromatogram in Figure 9.

Time (minutes)	Deionized H_2O	Oxalic acid	DAPA
0	20%	75%	5%
10	50%	25%	25%
20	50%	25%	25%
30	25%	25%	50%
40	25%	25%	50%
50	20%	75%	5%
60	20%	75%	5%

Table 3. Observed ratios vs. natural ratios and the percent recovery of the chosen analytes, separated using the oxalic acid and diaminopropanoic acid separation method

Element	Ratio	Natural ratio	Observed ratio	Percent recovery
Gadolinium	158/160	1.14	1.12	98%
Europium	151/153	0.92	0.89	97%
Samarium	149/152	0.52	0.51	98%
Neodymium	143/146	0.71	0.68	96%

3.1.3 Oxalic Acid and Diglycolic Acid

A second anionic separation was also tested. Oxalic acid (0.1 M, buffered to pH 4.5 using ammonium hydroxide) was used in conjunction with diglycolic acid (DGA, 0.1 M, buffered to pH 4.5 using ammonium hydroxide) and the multifunctional CS-5A Dionex resin. Figure 10 illustrates the resulting

chromatogram showing symmetrical peak shapes and quantitative separation for all analytes except for gadolinium. As with the HIBA and oxalic/DAPA methods, the isotopic ratios of the analyte lanthanides were within a few percent of known.

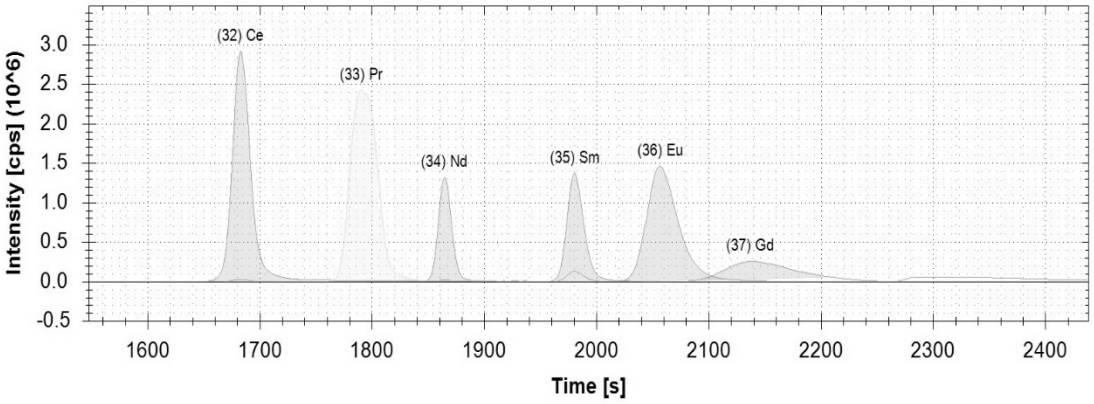

Figure 10. Anion exchange—using a mixed oxalic acid and diglycolic acid gradient elution (buffered with NH_4OH) as the mobile phase. Lanthanides elute in order of decreasing ionic radius and are measured as the chosen isotopic mass in the chromatogram.

3.1.4 Pyridine Dicarboxylic Acid (PDCA) Transition Metal Separation Scheme

Ammonium hydroxide buffered anionic and cationic lanthanide separation schemes have shown to be successful using the multifunctional CS-5A Dionex resin. The next stage was to test an existing eluent, pyridine dicarboxylic acid (PDCA) for a transition metal separation scheme. PDCA (0.006 M, buffered to pH 4.5 using ammonium hydroxide) was employed in an isocratic elution. Figure 11 illustrates the resulting chromatogram showing the separation of iron, nickel, copper, and manganese. The peak shapes are symmetrical, and the resolution is also good. In this proof of concept analysis, 25 ng of each analyte were injected as the transition metal masses tend to have a slightly higher background than observed for the lanthanide masses.

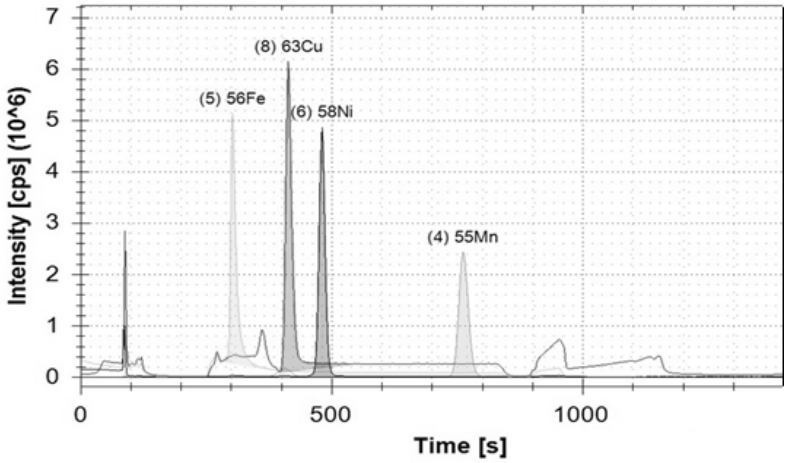

Figure 11. Transition metal separation using a pyridine dicarboxylic acid eluent (buffered with NH_4OH) as the mobile phase, measured as the chosen isotopic mass in the chromatogram.

3.2 CHOSEN SEPARATION SCHEME

To establish a separation method that will maximize the sample and minimize analysis time, a separation scheme was established that enabled the combination of the PDCA transition metal separation and the oxalic/DGA separation. The resulting analysis enabled the isobaric separation and quantitation of 26 elements of interest in potential post-detonation debris. Figure 12 shows a graphical representation of the eluent profile detailed in Table 4. The four eluents are deionized water (shown in the figure in yellow and used mainly as a diluent for the other eluents), 6 mM PDCA (shown in green and used for the transition metal separation), 100 mM oxalic acid (shown in pink), and 100 mM DGA (shown in blue and used in combination with oxalic acid for lanthanide separation and elution).

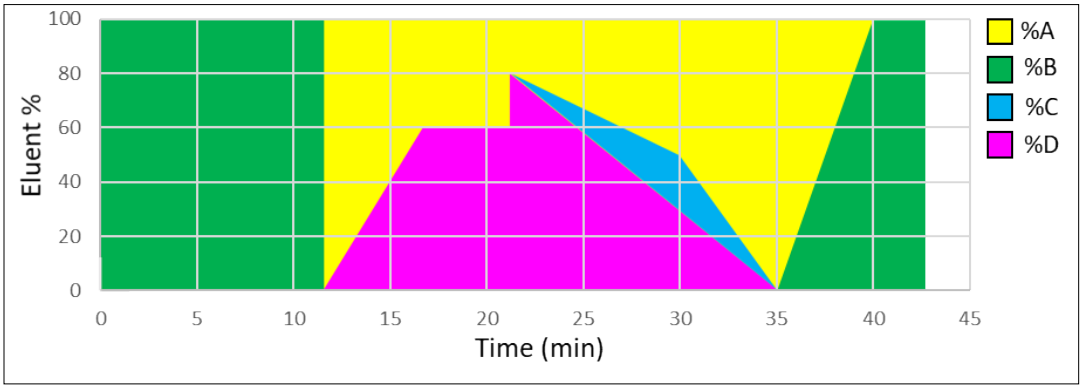

Figure 12. Gradient separation scheme using deionized water (yellow), 6 mM pyridine dicarboxylic acid (green), 100 mM oxalic acid (pink), and 100 mM diglycolic acid (blue).

Table 4. Time and percent contribution from each eluent for the separation scheme detailed in Figure 12

Time (minutes)	Deionized water (A, yellow in figure)	PDCA (6 mM) (B, green in figure)	DGA (100 mM) (C, lt. blue in figure)	Oxalic acid (D, pink in figure)
0	0%	100%	0%	0%
12	0%	100%	0%	0%
12.1	100%	0%	0%	0%
17	40%	0%	0%	60%
17.1	40%	0%	0%	60%
21	40%	0%	0%	60%
21.1	20%	0%	0%	80%
30	51%	0%	23%	26%
35	100%	0%	0%	0%
40	0%	100%	0%	0%
42	0%	100%	0%	0%

Notes: PDCA = pyridine dicarboxylic acid; DGA = diglycolic acid.

After the initial testing, a 5-minute washing period of 100% 100 mM oxalic acid took place to ensure any contaminants left on the resin were eluted. This was followed by a 5-minute washing period of 100% PDCA to remove any contaminants left from the oxalic acid in preparation for the following sample.

3.2.1 Reagents and Standards

Eluents for HPIC and all other solutions were prepared with trace metals basis grade chemicals and ultrapure water (18.2 MΩ cm) from a Millipore Milli-Q™ water purification system (Millipore). The following chemicals for eluents were dissolved in ultrapure water, then buffered with ammonium hydroxide (NH_4OH; 20–22% as NH_3; Trace Metal Grade Lot 7115080; Fisher Scientific, 1 Reagent Lane, Fair Lawn, NJ 07410) to a final pH of 4.5–4.8:

- Diglycolic acid ($C_4H_6O_5$; (recrystallized; >98% Lot A0353334; Acros Organics, New Jersey)
- 2,6-Pyridinedicarboxylic acid ($C_7H_5NO_4$; 99.999% metals basis Lot BCBQ3850V; Fluka, Sigma-Aldrich Co.)
- Glacial acetic acid ($C_2H_4O_2$; 99.99% trace metals basis Lot SHBH2511V; Sigma-Aldrich Co., 3050 Spruce Street, St. Louis, MO 63103)
- Oxalic acid ($C_2H_2O_4$; 99.999% trace metals basis Lot MKCC3466; Sigma-Aldrich Co.)

3.2.2 Chromatograms Produced Using the PDCA/DGA/Oxalic Acid Elution

The following chromatograms were produced by injecting 2.5 ng onto a CS_5A column and separated using the elution protocol detailed in section 3.2. As shown in Figure 13, there is a significant separation between the initial PDCA eluent and the DGA/oxalic acid eluent.

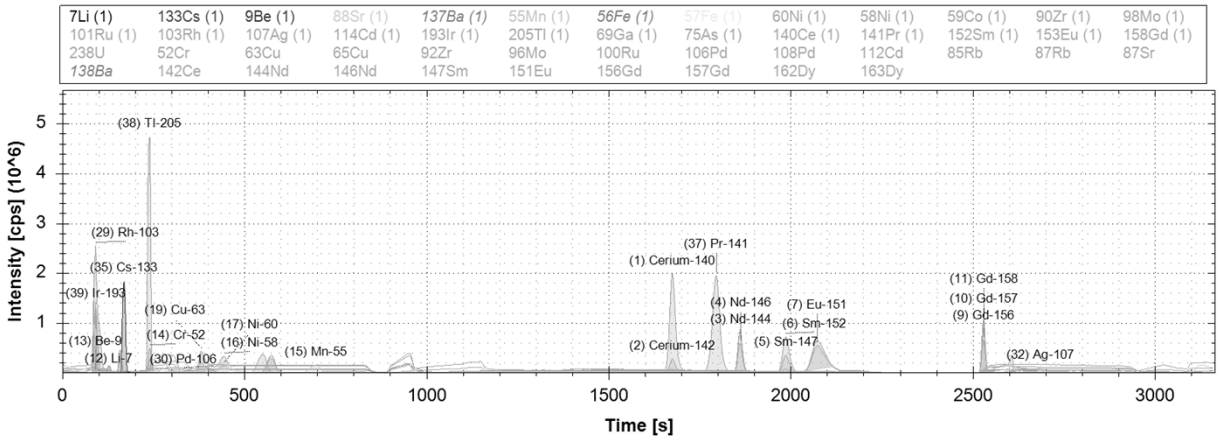

Figure 13. Complete chromatogram of 26 elements (39 isotopes).
Barium and iron traces have been removed for clarity.

Figures 14–16 show blown-up regions of the chromatogram illustrated in Figure 12, showing each of the individual analytes in more detail including isotopic sensitivity, peak shape, retention time, isobaric and elemental overlap, and peak tailing.

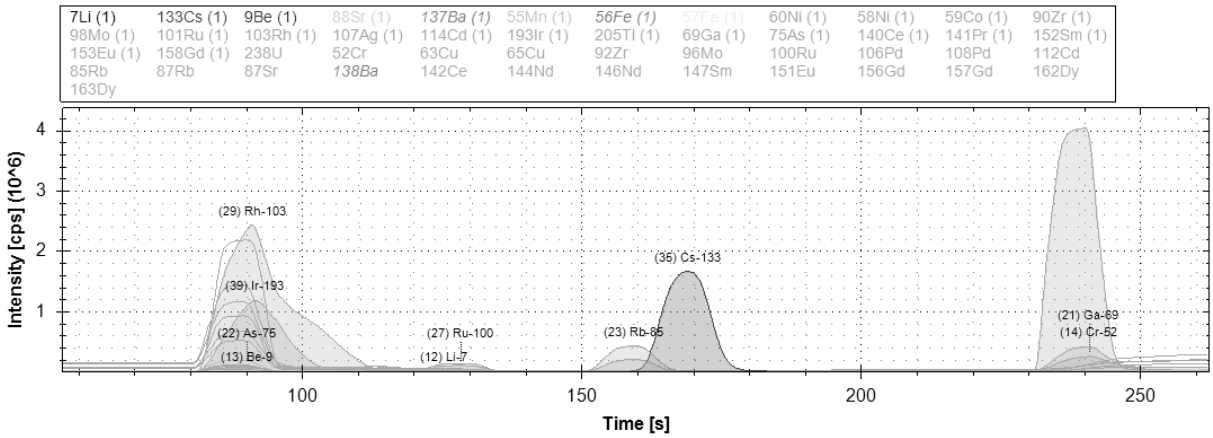

Figure 14. Partial chromatogram of the 0–250 second region, indicating the elution of the solvent front at around 90 seconds, followed by ruthenium and the group 1 metals, and finally by gallium, thallium, and chromium (iron omitted for clarity) at the 240 second mark.

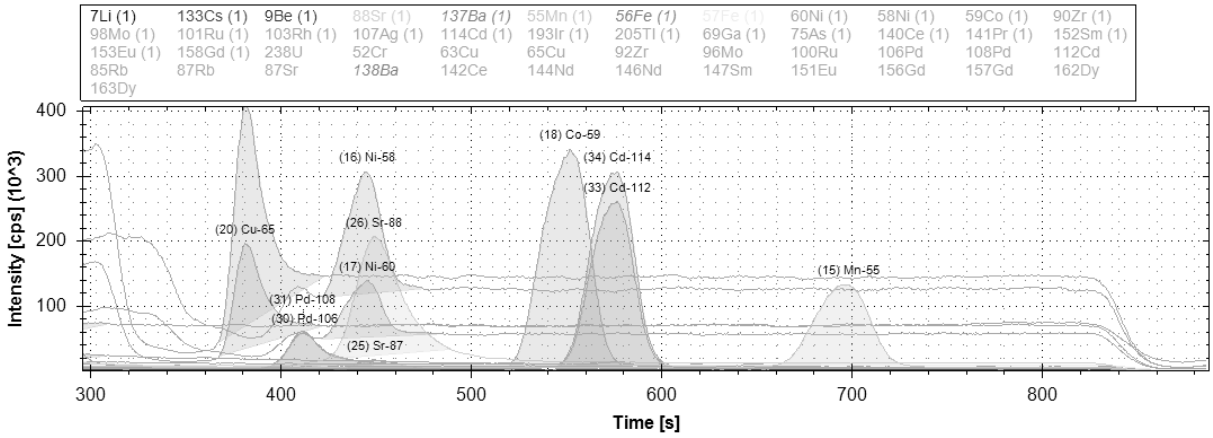

Figure 15. Partial chromatogram of the 300–900 second region, indicating the elution of the first row transition metals, together with strontium, palladium, and cadmium. Two isotopes of each element were monitored where possible.

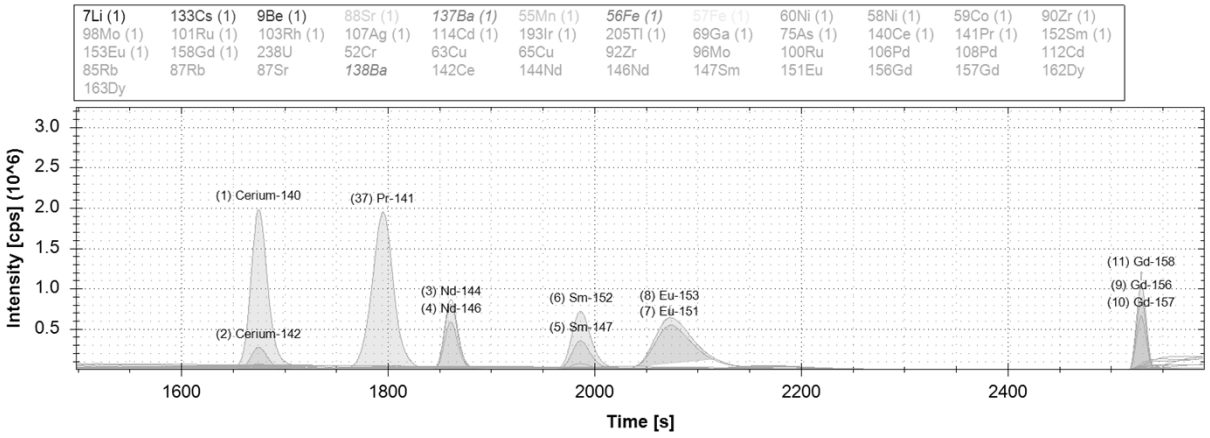

Figure 16. Partial chromatogram of the lanthanide region, indicating the separation of cerium, praseodymium, neodymium, samarium, europium, and gadolinium.
Two or three individual isotopes of each element were monitored.

4. METHOD STABILITY AND REPRODUCIBILITY

To determine the stability of the method with regard to both the chromatographic separation, defined as standard deviation of the retention time, and the peak shape and area reproducibility, seven replicates of a multielement standard (2.5 ng column load) were measured. Where possible, multiple isotopes of the same element were analyzed, enabling analysis of the reproducibility and accuracy of isotope ratios.

4.1 RETENTION TIMES AND PEAK REPRODUCIBILITY

Table 5 shows the retention times, average peak area, standard deviation, and relative standard deviation (RSD) for all the chosen isotopes. The retention times for all of the peaks are within 5 seconds throughout the 8 hour run; only lithium, europium, and praseodymium have a lower tolerance at 7 seconds. The reproducibility varies slightly, but most signal RSDs are ≤ 10%; only copper, chromium, and palladium are outside of this range, possibly because of the peak picking software not currently at an optimum for these elements.

Table 5. Retention times, average total counts, standard deviation (SD), and relative standard deviation (RSD) of seven replicates of a multielement standard

Isotope	Retention time (seconds)	Average area (counts)	SD (counts)	RSD
Ce-140	2070	3.39E+07	2.79E+06	8%
Ce-142	2070	4.67E+06	3.12E+05	7%
Nd-144	1862	1.18E+07	5.68E+05	5%
Nd-146	1862	8.60E+06	4.98E+05	6%
Sm-147	1990	6.95E+06	4.24E+05	6%
Sm-152	1990	1.45E+07	7.58E+05	5%
Eu-151	2070	1.56E+07	1.23E+06	8%
Eu-153	2070	1.88E+07	1.65E+06	9%
Gd-156	2531	9.75E+06	4.72E+05	5%
Gd-157	2531	7.37E+06	3.65E+05	5%
Gd-158	2531	1.16E+07	6.15E+05	5%
Li-7	129	2.70E+04	1.17E+03	4.3%
Be-9	90	6.41E+03	3.76E+02	6%
Cr-52	242	5.13E+06	6.42E+05	12%
Mn-55	695	4.02E+06	1.37E+05	3%
Ni-58	445	4.15E+06	1.76E+05	4%
Ni-60	445	1.88E+06	6.63E+04	4%
Co-59	553	9.50E+06	4.55E+05	5%
Cu-63	383	1.95E+06	1.32E+05	6.7%
Cu-65	383	6.73E+05	3.13E+04	4.6%
Ga-69	243	2.96E+06	1.87E+05	6%
As-75	92	9.64E+05	8.12E+04	8%
Rb-85	161	4.05E+06	1.77E+05	4%
Rb-87	161	1.88E+06	8.02E+04	4%
Sr-87	447	3.63E+05	1.77E+04	5%
Sr-88	447	5.06E+06	1.96E+05	4%
Ru-100	130	1.02E+06	5.46E+04	5%
Ru-101	130	1.37E+06	7.79E+04	6%
Rh-103	93	3.35E+07	1.68E+06	5%
Pd-106	411	8.98E+05	1.08E+05	12%
Pd-108	411	9.33E+05	1.20E+05	13%
Ag-107	2685	1.90E+06	2.04E+05	11%
Cd-112	576	6.64E+06	2.35E+05	4%
Cd-114	576	8.00E+06	3.29E+05	4%
Cs-133	171	1.60E+07	1.03E+06	6%
Pr-141	1795	4.49E+07	2.38E+06	5%
Tl-205	240	4.25E+07	2.07E+06	5%
Ir-193	92	1.40E+07	8.50E+05	6%

4.2 ISOTOPIC RATIO REPRODUCIBILITY AND RECOVERY

Although peak stability is important to ensure that the developed method is sufficiently robust, isotopic ratio stability is more important when IDMS is to be employed for quantitation. Table 6 details the average determined peak area ratios together with the standard deviaton and the relative standard deviation of seven replicates. The observed ratios of these natural standards are compared with the actual natural elemental mass ratios. The RSD for the majority of cases is < 2%; strontium and palladium are the exceptions but still showed < 4% RSD. The isotope ratio recoveries (observed atom % ratio/known mass % ratio) seem to be close to known, with the majority being within 10% of known. Even those with lower accuracy shouldn't pose an issue as the precision of the measurement is good enough to use a certified natural standard and mass correct. For accurate IDMS concentrations, a mass bias correction involves analyzing a standard of natural isotopic abundance alongside the samples, at a similar concentration. The recovery from the natural standard is determined, and the isotopic ratio of the sample is corrected

Table 6. Isotopic ratios derived from total counts for each isotope, standard deviation (SD), and the isotopic ratios from the seven replicates are shown together with the relative standard deviation (RSD) for clarity

The elemental mass ratio for the isotopic ratio is also given together with the recovery (observed atom % ratio/known mass % ratio)

Ratio	Average	SD	RSD	Element mass ratio	Recovery
Ce-140/Ce-142	7.194	0.119	1.7%	7.961	90.4%
Nd-144/Nd-146	1.387	0.014	1.0%	1.384	100.2%
Sm-147/Sm-152	0.480	0.005	1.1%	0.560	85.6%
Eu-151/Eu-153	0.828	0.013	1.5%	0.916	90.4%
Gd-156/Gd-157	1.323	0.006	0.4%	1.308	101.2%
Gd-157/Gd-158	0.633	0.009	1.3%	0.630	100.5%
Ni-58/Ni-60	2.182	0.041	1.9%	2.596	84.1%
Cu-63/Cu-65	2.145	0.049	2%	2.241	95.7%
Rb-85/Rb-87	2.150	0.018	0.8%	2.593	83%
Sr-87/Sr-88	0.072	0.003	3.7%	0.085	84.4%
Ru-100/Ru-101	0.721	0.014	2%	0.741	97.3%
Pd-106/Pd-108	0.964	0.024	2.4%	1.033	93.3%
Cd-112/Cd-114	0.830	0.009	1.1%	0.840	98.9%

5. METHOD LIMITS OF DETECTION AND QUANTITATION

The limits of detection (LOD) and quantitation (LOQ) for the individual isotopes were calculated using a linear regression slope analysis. A series of multielemental standards with column loading ranging from 25 pg to 2.5 ng was analyzed using the developed HPIC-ICPMS separation scheme. After the peak areas were determined using the Qtegra software, the data were exported to Microsoft Excel and, employing the Analysis Toolpak, linear regression analysis was carried out using the regression function. This yielded, among other information, the standard deviation of the y-intercept from a least-squares linear regression slope analysis. Multiplying by 3.3 yields the limit of detection of the isotope, and multiplying by a factor of 10 gives the limit of quantitation. For elements with multiple isotopes, the analyzed isotope was multiplied by the isotopic contribution to yield isotopic LOD and LOQ values, which will be important when employing enriched isotope standards for IDMS analyses.

Further weight for the LOQ values becomes apparent when looking at the isotopic ratios of the standards close in concentration to the LOQ level. For many of the analytes, the measured isotopic ratio at the LOQ was within 3% of that measured at 1.25 ng. The measured ratios at the LOQ were also shown to be within 5–10% of known.

Obviously, these values have been determined for an ideal system with varying matrices and acid concentrations likely having a negative effect for real systems, yielding higher LODs and LOQs. These values do, however, give weight to the overall sensitivity of the analytical method.

Tables 7 and 8 detail the LOD and LOQ for the individual isotopes monitored for the lanthanide elements and the groups I and II elements, respectively. Table 9 shows the LOD and LOQ for the individual isotopes monitored for the first-row transition metal elements with gallium and arsenic, and Table 10 shows the LOD and LOQ values for the individual isotopes monitored for the second row transition metal elements with cadmium, iridium, and thallium.

Table 7. The limits of detection (LOD) and quantitation (LOQ) for the individual isotopes monitored for the lanthanide elements
The elemental LOD and LOQ refer to the calculated numbers based on a linear regression slope analysis,[a] and the isotopic LOD and LOQ are calculated by multiplying the isotopic numbers by the natural isotopic abundance. Also detailed are the determined isotopic ratios of the standard closest to the LOQ level (for the lanthanide isotopes, this was the 25 pg standard), together with the percent recovery from known and the percent recovery from the 1.25 ng standard (which would be employed as a mass bias standard if isotope dilution mass spectrometry were to be employed)

Isotope	**Ce-140**	**Ce-142**	**Pr-141**	**Nd-142**	**Nd-144**	**Nd-146**	**Sm-147**	**Sm-152**
Elemental LOD (pg)	9.2	5.3	25.9	1.5	7.7	7.5	14.5	19.6
Elemental LOQ (pg)	27.8	16.1	78.5	4.5	23.4	22.8	44.0	59.3
Natural isotopic abundance	0.885	0.111	1.000	0.271	0.238	0.172	0.150	0.267
Isotopic LOD (pg)	8.1	0.6	25.9	0.4	1.8	1.3	2.2	5.2
Isotopic LOQ (pg)	24.6	1.8	78.5	1.2	5.6	3.9	6.6	15.8
Ratio	**Ce-140/Ce-142**			**Nd-142/Nd-144**	**Nd-142/Nd-146**		**Sm-147/Sm-152**	
Closest ratio to LOQ	7.48			1.10	1.54		0.46	
Natural ratio	7.99			1.14	1.58		0.56	
% recovery from 1.25 ppb ratio	97%			104%	106%		92%	
% recovery from natural ratio	94%			97%	97%		81%	

Isotope	**Eu-151**	**Eu-153**	**Gd-156**	**Gd-157**	**Gd-158**
Elemental LOD (pg)	2.8	3.8	12.4	15.0	9.0
Elemental LOQ (pg)	8.5	11.5	37.6	45.3	27.1
Isotopic abundance (%)	0.478	0.522	0.205	0.157	0.248
Isotopic LOD (pg)	1.3	2.0	2.5	2.3	2.2
Isotopic LOQ (pg)	4.0	6.0	7.7	7.1	6.7
Ratio	**Eu-151/Eu-153**		**Gd-156/Gd-157**	**Gd-156/Gd-158**	
Closest ratio to LOQ	0.86		1.25	0.78	
Natural ratio	0.92		1.31	0.82	
% recovery from 1.25 ppb ratio	98%		97%	97%	
% recovery from natural ratio	94%		96%	95%	

[a]The standard deviation of the y-intercept (y) and the slope of the linear regression line (x) were calculated using the Regression Function in the Data Analysis tool in Microsoft Excel. The LOD is defined as 3.3×(y/x), and the LOQ is defined as 10×(y/x).

Table 8. The limits of detection (LOD) and quantitation (LOQ) for the individual isotopes monitored for the groups I and II elements
The elemental LOD and LOQ refer to the calculated numbers based on a linear regression slope analysis,[a] and the isotopic LOD and LOQ are calculated by multiplying the isotopic numbers by the natural isotopic abundance. Also detailed are the determined isotopic ratios of the standard closest to the LOQ level (for rubidium, this was the 25 pg standard, and for strontium, it was the 250 pg standard), together with the percent recovery from known and the percent recovery from the 1.25 ng standard (which would be employed as a mass bias standard if isotope dilution mass spectrometry were to be employed)

Isotope	**Li-7**	**Rb-85**	**Rb-87**	**Cs-133**	**Be-9**	**Sr-87**	**Sr-88**
Elemental LOD (pg)	52.3	9.7	10.2	8.5	90.4	57.5	44.9
Elemental LOQ (pg)	158.4	29.3	31.0	25.7	274.0	174.3	136.1
Isotopic abundance (%)	0.925	0.722	0.278	1.000	1.000	0.070	0.826
Isotopic LOD (pg)	48.4	7.0	2.8	8.5	90.4	4.0	37.1
Isotopic LOQ (pg)	146.5	21.1	8.6	25.7	274.0	12.2	112.4
Ratio		**Rb-85/Rb-87**				**Sr-87/Sr-88**	
Closest ratio to LOQ		2.27				0.06	
Natural ratio		2.59				0.08	
% recovery from 1.25 ppb ratio		104%				90%	
% recovery from natural ratio		88%				71%	

[a]The standard deviation of the y-intercept (y) and the slope of the linear regression line (x) were calculated using the Regression Function in the Data Analysis tool in Microsoft Excel. The LOD is defined as 3.3×(y/x), and the LOQ is defined as 10×(y/x).

Table 9. The limits of detection (LOD) and quantitation (LOQ) for the individual isotopes monitored for the first row transition metal elements with gallium and arsenic

The elemental LOD and LOQ refer to the calculated numbers based on a linear regression slope analysis,[a] and the isotopic LOD and LOQ are calculated by multiplying the isotopic numbers by the natural isotopic abundance. Also detailed are the determined isotopic ratios of the standard closest to the LOQ level, together with the percent recovery from known and the percent recovery from the 1.25 ng standard (which would be employed as a mass bias standard if isotope dilution mass spectrometry were to be employed)

Isotope	**Mn-55**	**Co-59**	**Ni-58**	**Ni-60**	**Cu-63**	**Cu-65**	**Ga-69**	**As-75**
Elemental LOD (pg)	83.6	14.1	**248.5**	**292.8**	158.3	140.6	35.6	19.4
Elemental LOQ (pg)	253.2	42.6	**753.1**	**887.3**	479.7	426.1	107.9	58.7
Isotopic abundance (%)	1.000	1.000	0.683	0.261	0.692	0.309	0.601	1.000
Isotopic LOD (pg)	83.6	14.1	169.7	76.4	109.5	43.5	21.4	19.4
Isotopic LOQ (pg)	253.2	42.6	514.1	231.6	331.8	131.8	64.8	58.7
Ratio			**Ni-58/Ni-60**		**Cu-63/Cu-65**			
Closest ratio to LOQ			2.54		2.27			
Natural ratio			2.62		2.24			
% recovery from 1.25 ppb ratio			105%		99%			
% recovery from natural ratio			97%		101%			

[a]The standard deviation of the y-intercept (y) and the slope of the linear regression line (x) were calculated using the Regression Function in the Data Analysis tool in Microsoft Excel. The LOD is defined as 3.3×(y/x), and the LOQ is defined as 10×(y/x).

Table 10. The limits of detection (LOD) and quantitation (LOQ) for the individual isotopes monitored for the second row transition metal elements with cadmium, iridium, and thallium

The elemental LOD and LOQ refer to the calculated numbers based on a linear regression slope analysis,[a] and the isotopic LOD and LOQ are calculated by multiplying the isotopic numbers by the natural isotopic abundance. Also detailed are the determined isotopic ratios of the standard closest to the LOQ level, together with the percent recovery from known and the percent recovery from the 1.25 ng standard (which would be employed as a mass bias standard if isotope dilution mass spectrometry were to be employed)

ISOTOPE	Ru-100	Ru-101	Rh-103	Pd-106	Pd-108	Cd-112	Cd-114	Ir-193	Tl-205
Elemental LOD (pg)	39.7	33.0	16.6	23.8	24.0	24.3	25.1	10.1	17.0
Elemental LOQ (pg)	120.4	99.9	50.2	72.3	72.6	73.6	76.1	30.5	51.6
Isotopic abundance (%)	0.126	0.170	1.000	0.273	0.117	0.241	0.287	0.627	0.705
Isotopic LOD (pg)	5.0	5.6	16.6	6.5	2.8	5.9	7.2	6.3	12.0
Isotopic LOQ (pg)	15.2	17.0	50.2	19.7	8.5	17.8	21.9	19.1	36.4
RATIO	**Ru-100/Ru-101**			**Pd-106/Pd-108**		**Cd-112/Cd-114**			
Closest ratio to LOQ	0.71			1.03		0.83			
Natural ratio	0.74			1.03		0.84			
% recovery from 1.25 ppb ratio	101%			106%		102%			
% recovery from natural ratio	96%			100%		99%			

[a]The standard deviation of the y-intercept (y) and the slope of the linear regression line (x) were calculated using the Regression Function in the Data Analysis tool in Microsoft Excel. The LOD is defined as 3.3×(y/x), and the LOQ is defined as 10×(y/x).

6. APPLICATION OF DEVELOPED SEPARATION SCHEME TO ACTINIDE ELEMENTS

A multi-isotope spike of the elements listed in Table 11 was separated using the developed chemistry with the primary goal to ensure that it was also suitable for separation of the actinide elements.

Table 11. Isotopes incorporated in actinide spike

Element	Isotopes
Thorium	232
Uranium	233, 238
Neptunium	237
Plutonium	239, 240
Americium	241, 243
Curium	244, 246, 248

Uranium and neptunium appeared to elute successfully at the solvent front using the developed chemistry with americium and curium co-eluting as anionic complexes at the same time as the lanthanide elements. Plutonium and thorium, however, did not elute with the current chemistry.

By increasing the diglycolic acid concentration before the column cleaning protocol, the tetravalent actinides were also eluted, likely as the neutral bisdyglacolate species $[(Ac^{4+})(DGA^{2-})_2]^0$. The modified elution chemistry will be covered in more detail in Section 2.1 of an accompanying report, "Demonstration of a Rapid HPLC-ICPMS Direct Coupling Technique Using IDMS—Project Report: Part II."

Initially uranium appeared to elute at the solvent front, although it did not appear to be quantitative, and the isotopic composition of the spike wasn't recoverable, indicating the possible presence of trace U-238 contamination (see Figure 17). This is to be expected because under the current conditions, uranium should elute neither in the cationic PDCA separation nor in the anionic oxalic/diglycolic acid, and uranium will likely require the implementation of a fifth eluent of either 0.1 N nitric acid or 0.1 N hydrochloric acid.

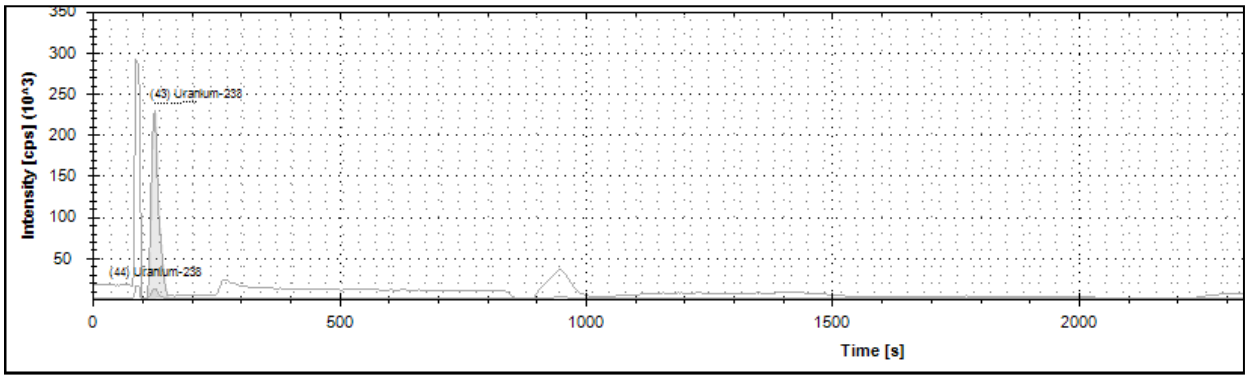

Figure 17. Chromatogram of m/z 238, indicating trace natural uranium in the injection system.

Neptunium and plutonium are likely to be present in multiple oxidation states in many dissolution matrices. This is apparent in Figure 18, where the majority of the neptunium elutes in the +5 oxidation state at the solvent front, albeit with significant peak tailing, and also in the +6 and +4 oxidation states. The addition of trace H_2O_2 to the sample before injection would drive 99%+ of the Np into the

+4 oxidation state (if the carrier acid was 6N-8N HNO_3), although the varying eluent chemistries may alter the oxidation state during sample elution.

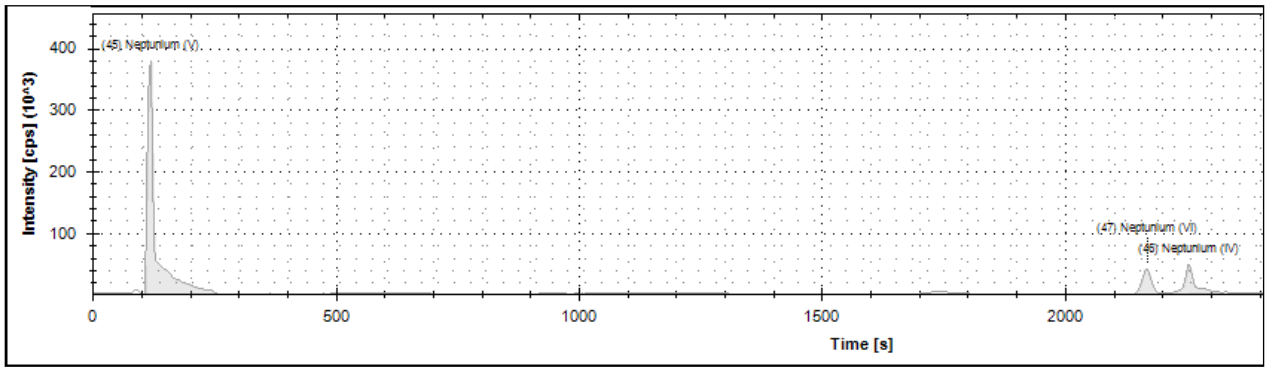

Figure 18. Chromatogram of m/z 237, showing the three distinct elution times of neptunium.

The chromatograms of curium and americium (Figure 19) were extremely similar in shape, width, and elution time. There is also significant peak overlap, so differentiation between Am-242 and Cm-242 and Am-243 and Cm-243 may be an issue using the current elution profile

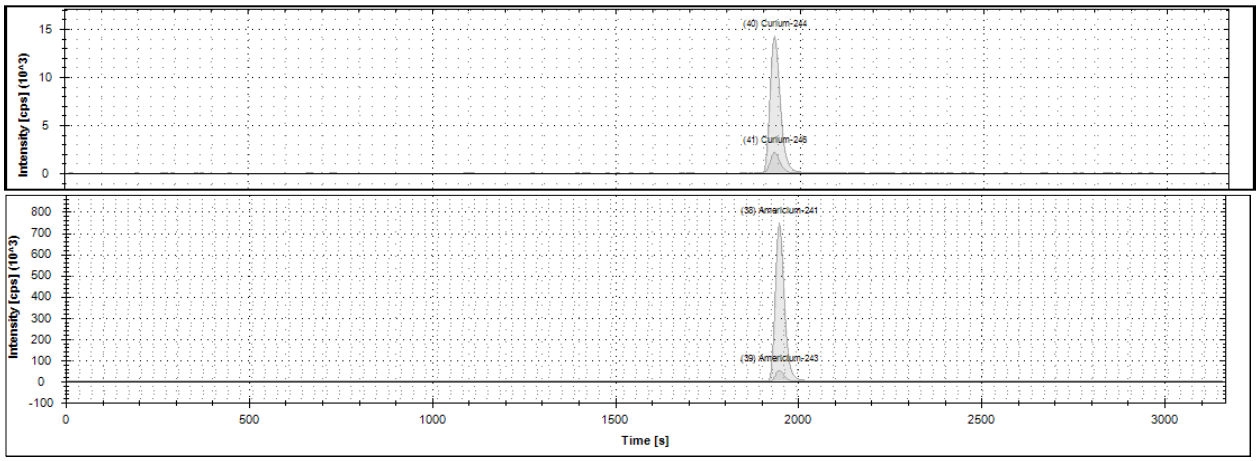

Figure 19. Chromatogram of m/z 244 and 248 (top) and m/z 241 and 243 (bottom), confirming the single elution times for curium and americium, respectively.

The modified elution protocol enabled the successful elution of the tetravalent actinides thorium and plutonium (Figure 20) as a single peak, although the plutonium does show slight peak tailing. Both thorium and plutonium are successfully separated from all isobaric interferences.

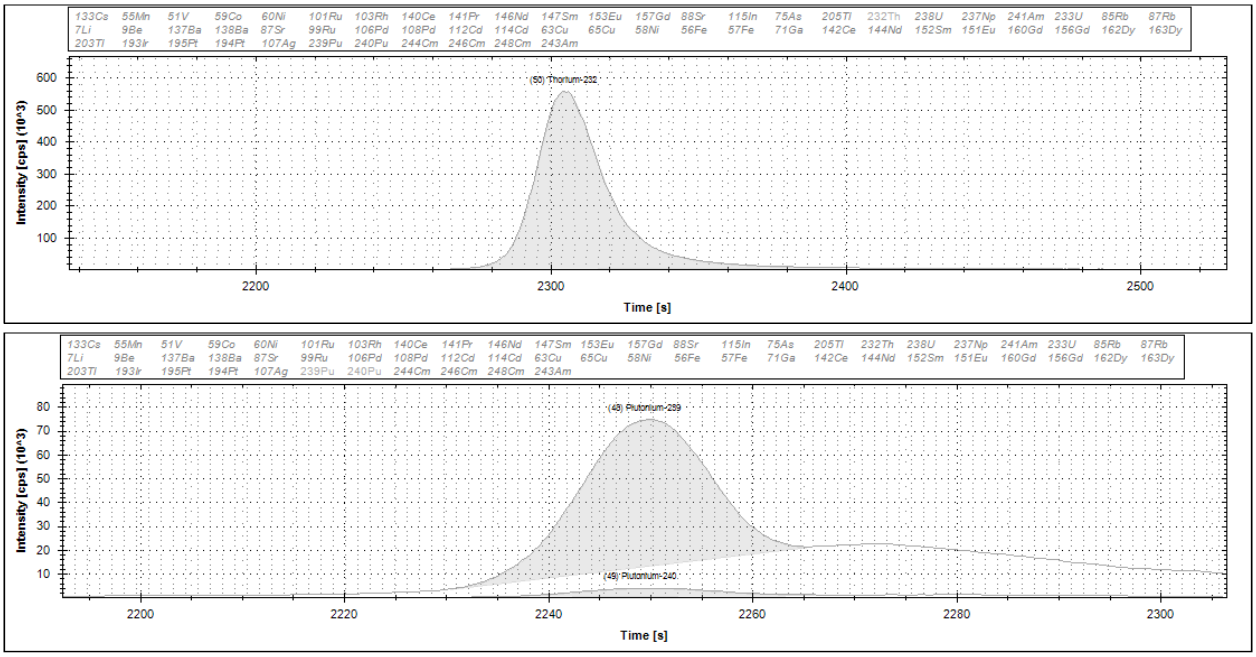

Figure 20. Chromatogram of m/z 232 (top) and m/z 240 and 239 (bottom), confirming the single elution times for thorium and plutonium, respectively.

7. FUTURE METHOD DEVELOPMENT

7.1 OVERCOMINING COMPLEX MATRICES

The next stage in method development will be to apply the current method to synthetic glass samples doped with trace impurities. For the method to be successful in the analysis of post detonation materials, it must be robust enough to be able to overcome the highly complex matrices of potential samples. The initial sample type to be investigated will be synthetic glass, doped with ng levels of specific elements, composed primarily of oxygen, silicon, aluminum, iron, and calcium (see Table 12). The majority of these components should elute at the solvent front, should not dramatically affect separation, and shouldn't be too much of a contamination concern for the mass spectrometer.

Table 12. Elemental composition of synthetic glass

Element	Approximate weight fractions
Silicon	26.90%
Aluminum	8.50%
Calcium	7.49%
Potassium	3.94%
Sodium	1.00%
Iron	1.64%
Magnesium	0.62%
Titanium	0.31%
Oxygen	49.60%

Source: J. J. Molgaard, et. al., "Development of Synthetic Nuclear Melt Glass for Forensic Analysis," *Journal of Radioanalytical and Nuclear Chemistry* 304, no. 3 (2015): 1293–1301.

7.2 INCORPORATING ISOTOPE DILUTION MASS SPECTROMETRY (IDMS)

IDMS employs a certified enriched isotope of an element of interest to determine the concentration of the analyte. In IDMS, certified enriched isotopes of each element of interest will be added directly into the sample matrix to be analyzed. This negates the need for external calibrations, thus reducing the analytical uncertainty. All additions and dilutions of standards and unknowns are performed gravimetrically to minimize analytical uncertainties. The resultant equilibrated mixtures and portions of the unknowns will be separated efficiently using the developed separation scheme and analyzed using ICPMS employing isotope ratio mass spectrometry (IRMS) for isotopic distributions. IRMS provides the most accurate and precise measurements available to analytical laboratories today. Each element's measured isotopic change between the unknown and the mixture is then used to calculate its concentration mathematically with a high degree of precision.

8. CONCLUSION

In conclusion, researchers have developed a robust and sensitive method to determine the concentration and isotopics of over 25 elements in a single analysis. The method robustness was proven over an 8 hour period yielding standard deviations of around 5%, isotopic ratio standard deviations of < 2%, and, on average, 98% recovery of isotopic ratios from known. The sensitivity of the analysis is comparable to many higher resolution sector mass spectrometers (using direct injection) with the majority of the limits of detection in the low picogram range. More importantly, the comparison of the determined isotopic ratios to natural ratios at the limit of quantitation yielded 95%+ recovery.

With further method development to determine the influence of matrices on the LOD, LOQ, separation, and robustness of the analysis, this technique has the potential to give rapid, precise analyses of post detonation materials using very little material.

9. REFERENCES

1. J. Giaquinto and B. Roach, *Phase II Proposal Title: Demonstration of a Rapid HPLC-ICPMS Direct Coupling Technique Using IDMS*, DTRA J9-NTFC/A FY15 Solicitation, Oak Ridge National Laboratory, Oak Ridge, Tenn., 2015.
2. I. C. Gauld, J. M. Giaquinto, J. S. Delashmitt, J. Hu, G. Ilas, T. J. Haverlock, and C. Romano, "Re-evaluation of Spent Nuclear Fuel Assay Data for the Three Mile Island Unit 1 Reactor and Application to Code Validation," *Annals of Nuclear Energy* 87, part 2 (January 2016): 267–281.
3. "Ion Chromatography of Lanthanide Metals," Dionex France, August 1991, http://www.dionex-france.com/library/literature/technical_notes/TN23_LPN032889-01.pdf.
4. "IonPac ® CS5A Column & MetPac ™ Reagents," Dionex Corporation, July 2001, http://www.dionex.com/en-us/webdocs/4263-DS_IonPac_CS5A_LPN0745-03.pdf.
5. "Product Manual," Dionex Corporation, November 2002, http://www.dionex.com/en-us/webdocs/4342-31188-06_CS5A_V17.pdf.

APPENDIX A. PEAK ELUTION CHROMATOGRAMS

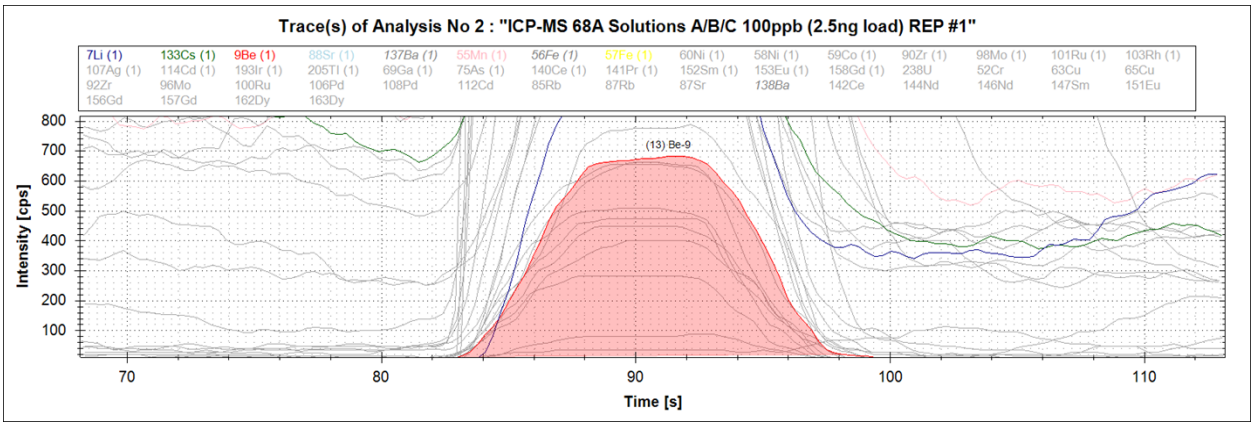

Figure A-1. Elution of beryllium, showing a fairly symmetrical peak, although not gaussian distribution, with significant elemental overlap. Peak shape is likely due to solvent front elution.

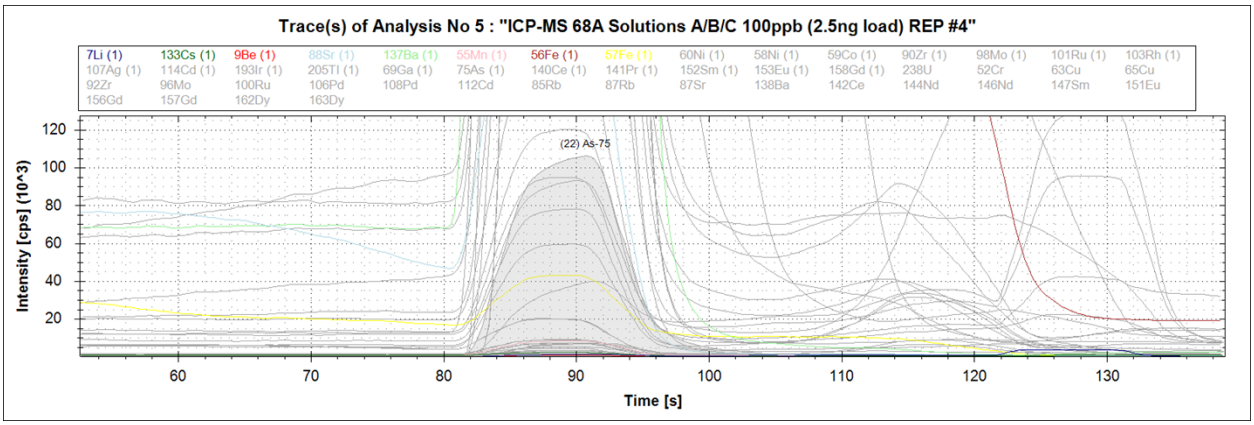

Figure A-2. Elution of arsenic, showing a nonsymmetrical peak, with significant elemental overlap. Peak shape is likely due to solvent front elution.

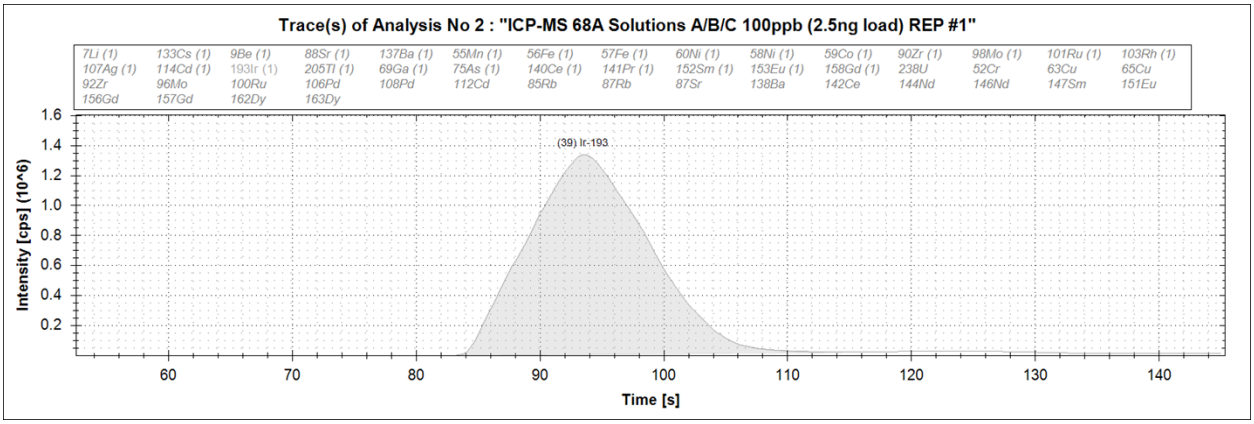

Figure A-3. Elution of iridium, showing a nonsymmetrical peak, with significant elemental but no isobaric overlap. Slight tailing is visible, with peak shape likely due to solvent front elution.

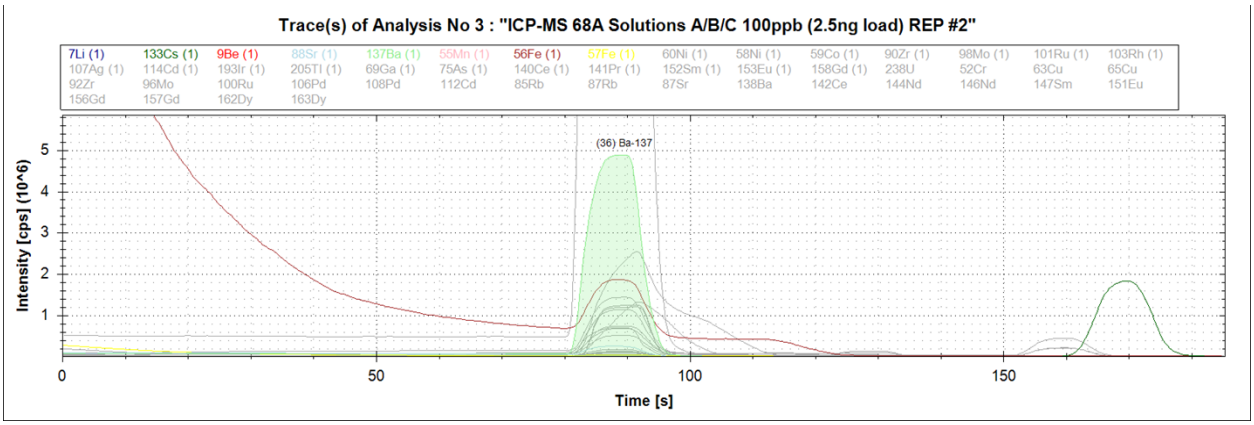

Figure A-4. Elution of barium, showing a very intense peak, with significant elemental but no isobaric overlap. Peak shape is likely due to solvent front elution; very good separation from cesium is shown.

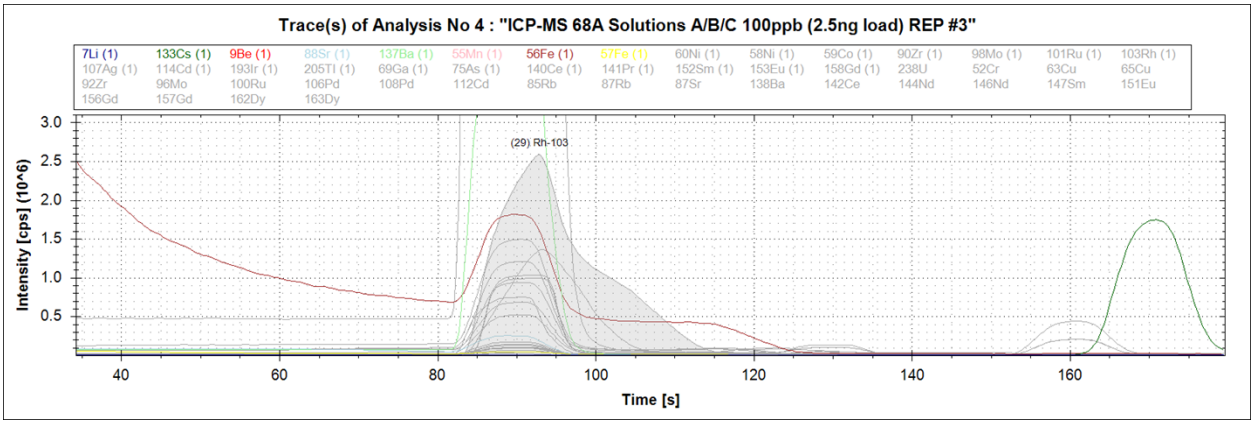

Figure A-5. Elution of rhodium, showing a nonsymmetrical peak, with significant elemental overlap. Peak shape is likely due to solvent front elution and potential column redox.

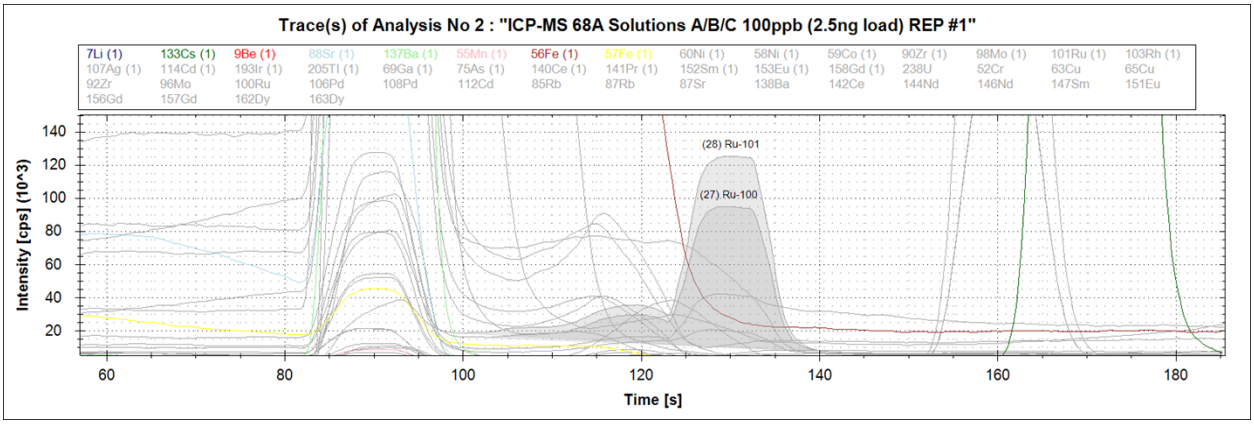

Figure A-6. Elution of ruthenium, showing a nonsymmetrical peak, with significant elemental but no isobaric overlap. Peak shape is likely due to solvent front elution, potential column redox, and low intensity. Peak may require a different peak picking protocol to decrease the allowed baseline window to < 50 seconds

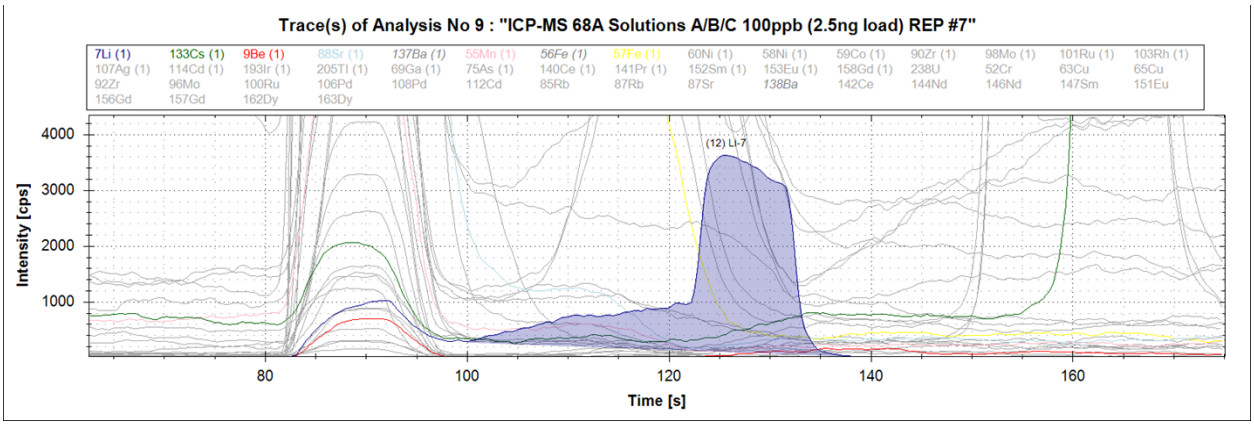

Figure A-7. Elution of lithium, showing a nonsymmetrical peak with significant elemental overlap. Peak shape is likely due to solvent front elution and low intensity. Peak requires a different peak picking protocol to decrease the allowed baseline window to < 50 seconds

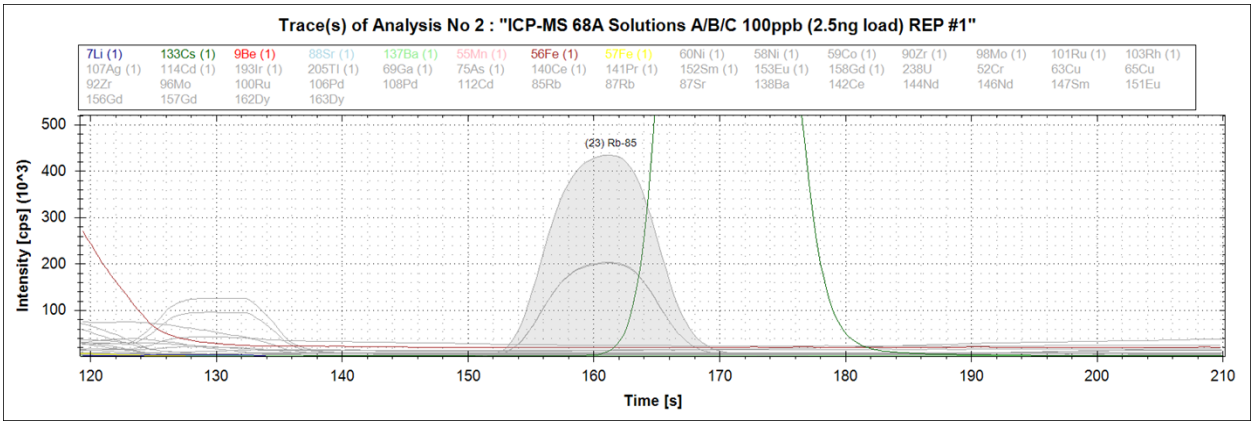

Figure A-8. Elution of rubidium, showing a very symmetrical gaussian distribution with little elemental and no isobaric (strontium) overlap.

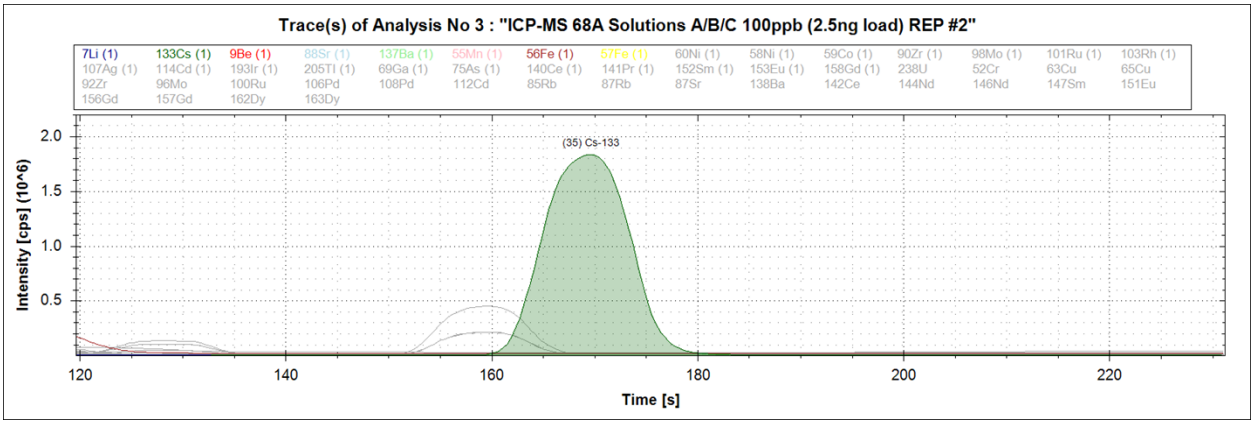

Figure A-9. Elution of cesium, showing a very symmetrical gaussian distribution with little elemental and no isobaric (barium on radioactive Cs-137) overlap.

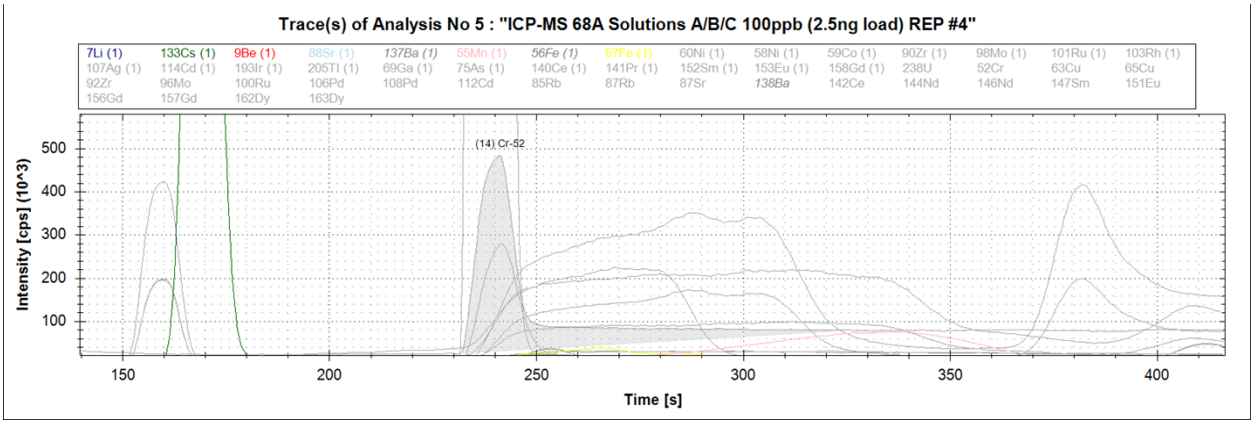

Figure A-10. Elution of chromium, showing significant tailing and potential isobaric interferences from iron.

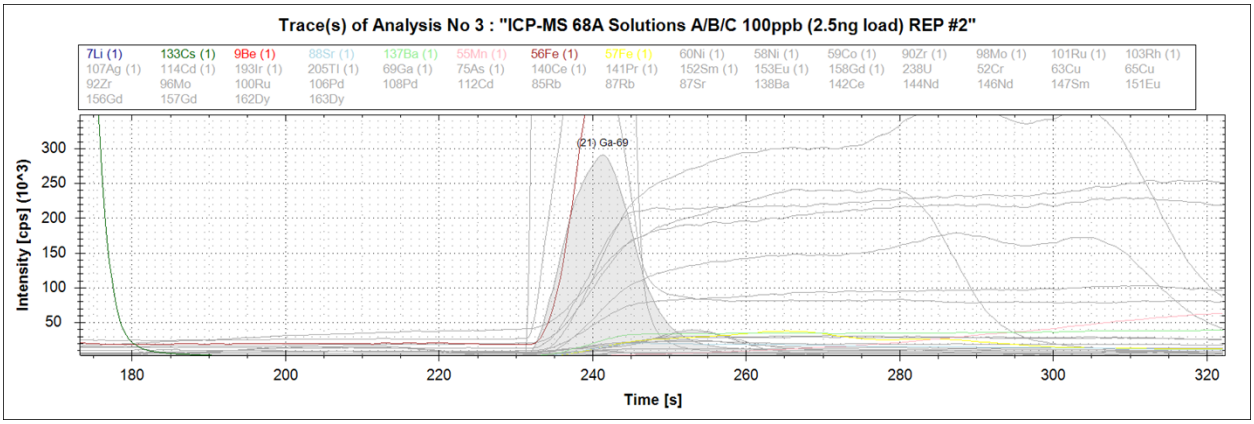

Figure A-11. Elution of gallium, showing a very symmetrical gaussian distribution with significant elemental but no isobaric overlap.

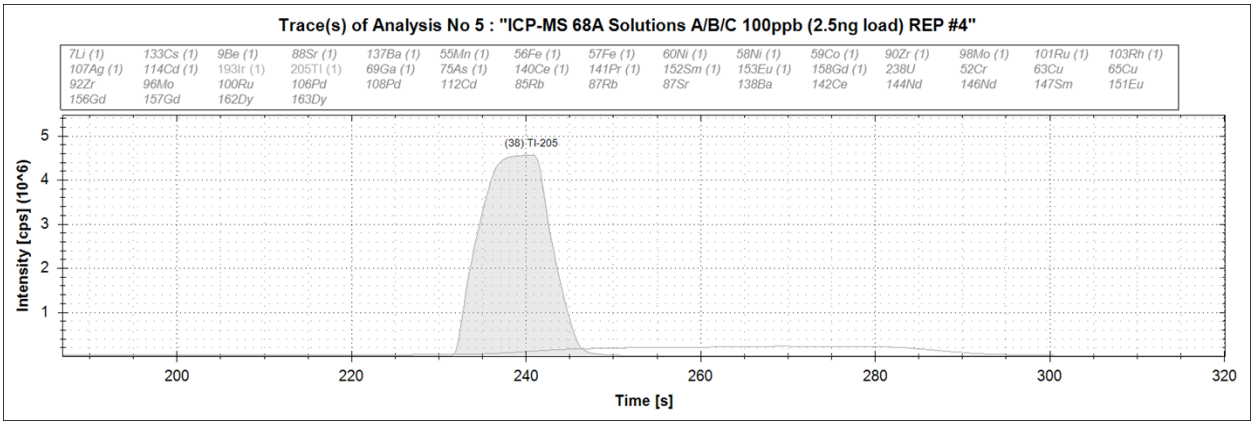

Figure A-12. Elution of thallium, showing an intense peak with elemental but no isobaric overlap.

The first row transition metals do separate; however, there seems to be significant tailing of the peaks. At these lower levels, this tailing is fairly significant, in particular for iron and copper.

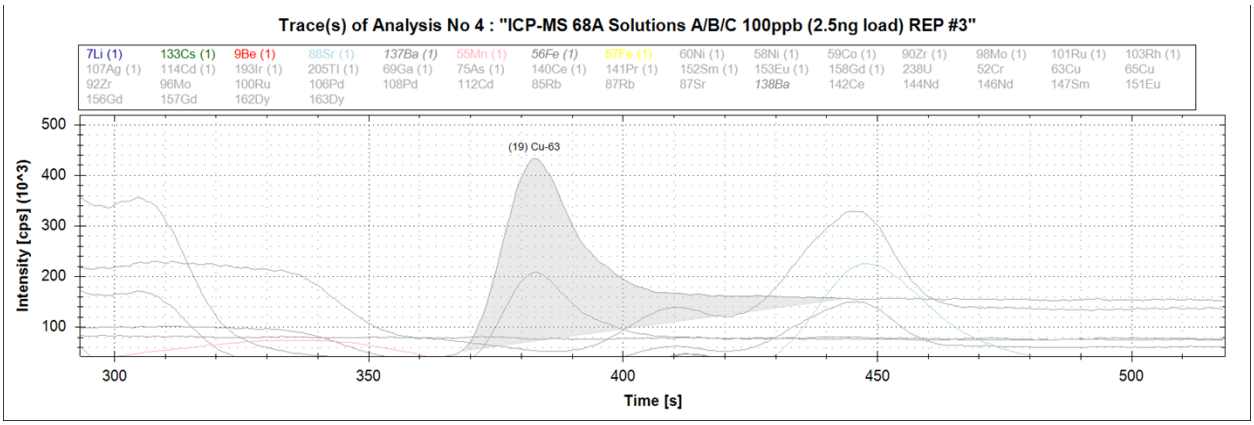

Figure A-13. Elution of copper, showing a low intensity peak with elemental overlap and tailing, could cause issues if Ni-63 is a target isotope, as natural copper would surely suppress the signal.

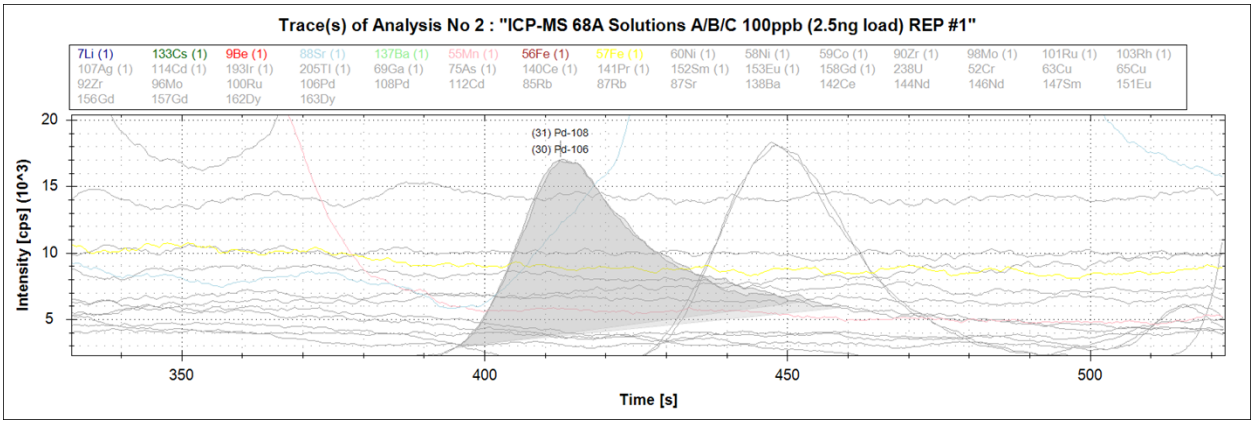

Figure A-14. Elution of palladium, showing a low intensity peak with elemental overlap and tailing, should not cause issues if Cd 106, 108, and 110 are the target isotopes, because the signal is significantly weaker than observed for cadmium.

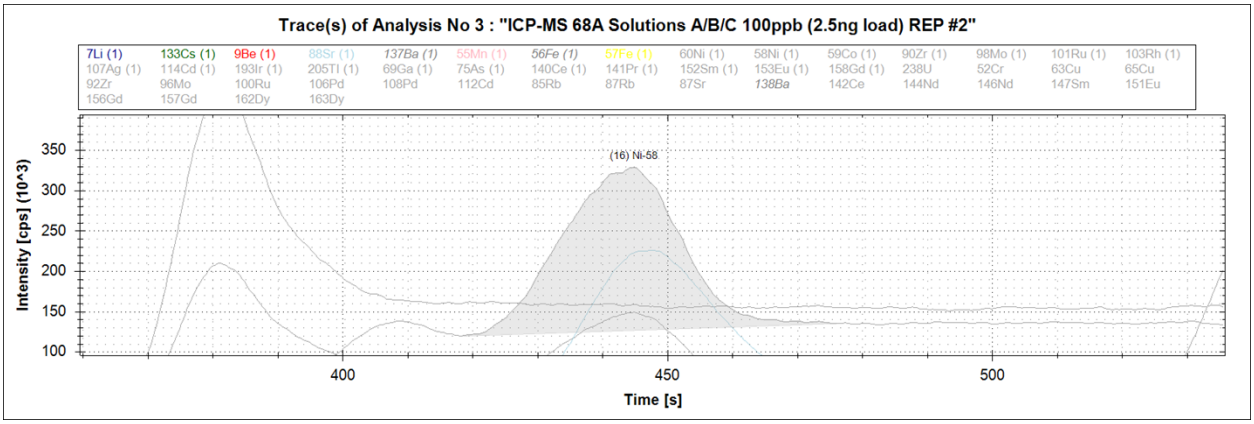

Figure A-15. Elution of nickel, showing a low intensity peak with elemental overlap.

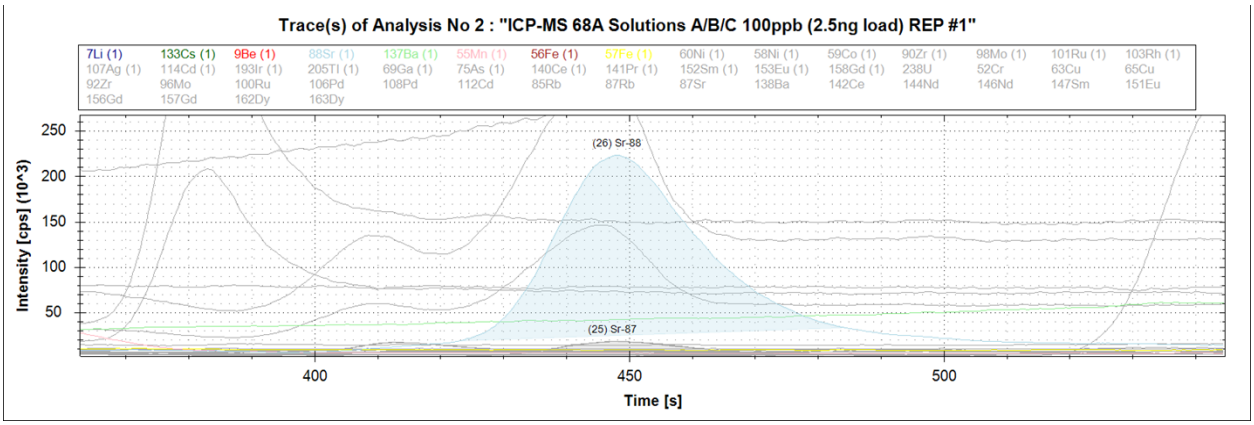

Figure A-16. Elution of strontium, a clean peak with elemental but no isobaric overlap—separated from rubidium and zirconium, which is important if Sr-90 is an analyte.

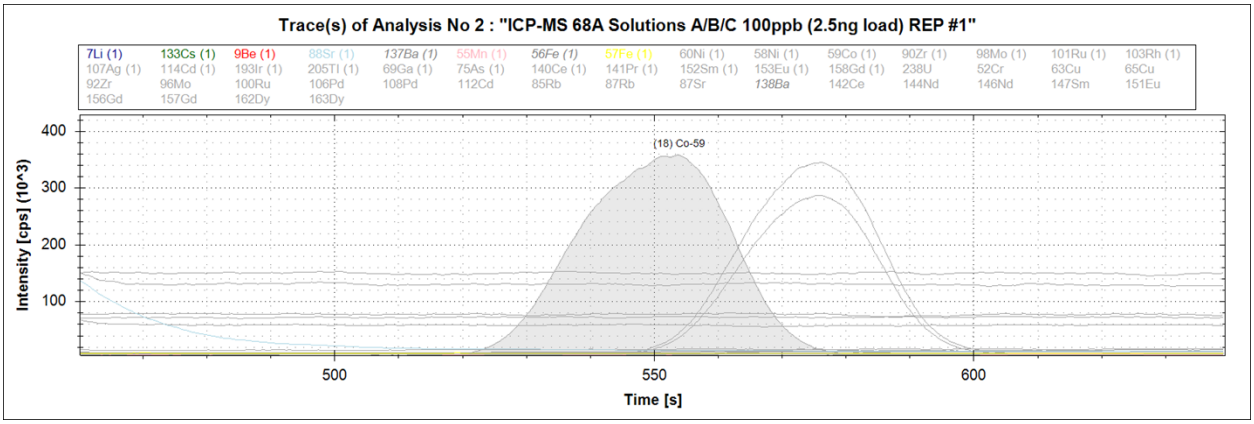

Figure A-17. Elution of cobalt, a clean peak with slight elemental but no isobaric overlap and minimal tailing; good separation from nickel is shown, which is important if Co-60 is an analyte.

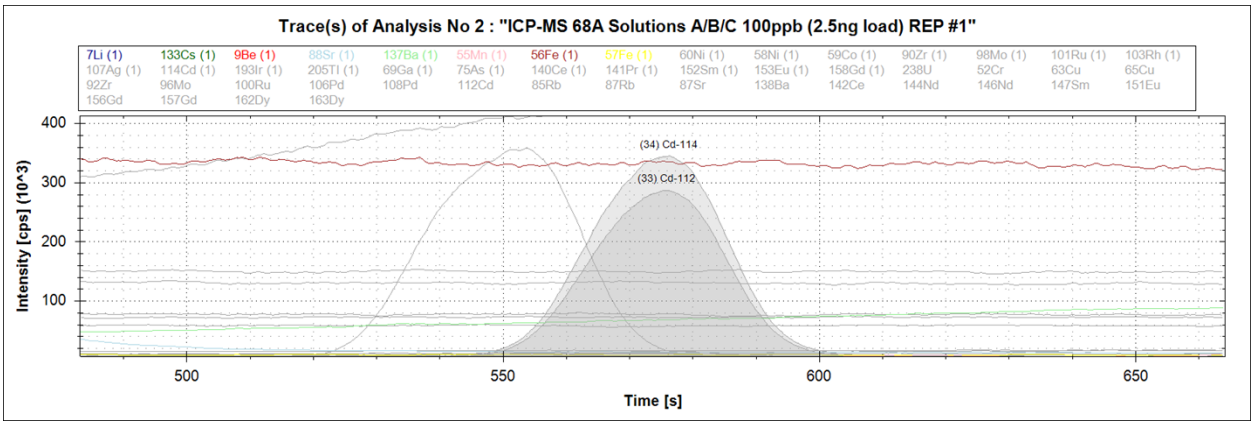

Figure A-18. Elution of cadmium, a clean peak with good symmetry, no tailing, and slight elemental overlap. No isobaric overlap is assumed (although tin is not monitored; it may elute at 115 s as slight signal of 114 is visible at this elution time).

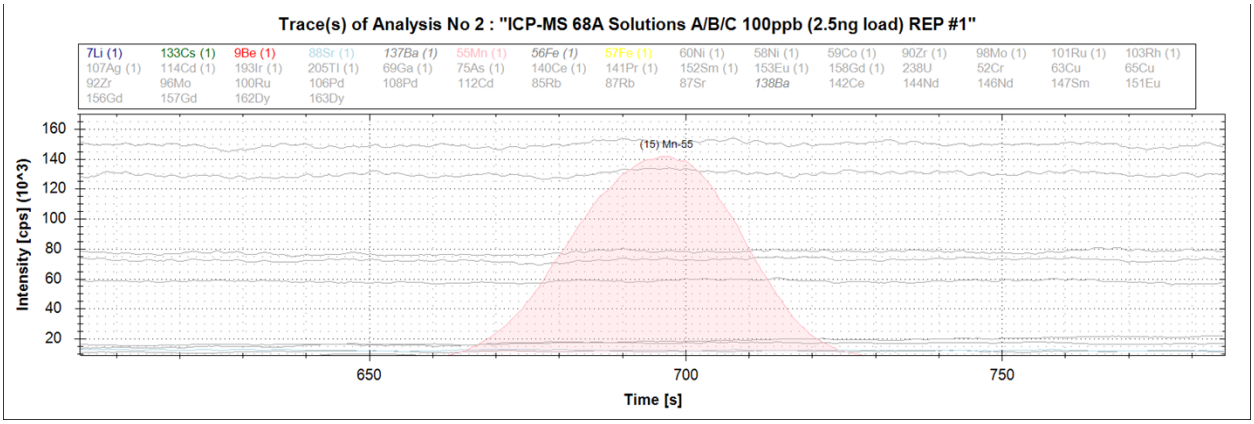

Figure A-19. Elution of manganese, a clean peak with good symmetry and little elemental overlap. No isobaric overlap is assumed, and separation from iron is enough that Mn-55 won't interfere with Fe-55 analysis.

The lanthanide region, using the oxalic acid/diglycolic acid elution system, shows very clean peaks, with good baselines and potentially very low detection limits. The peaks have high symmetry and result in very precise isotopic data.

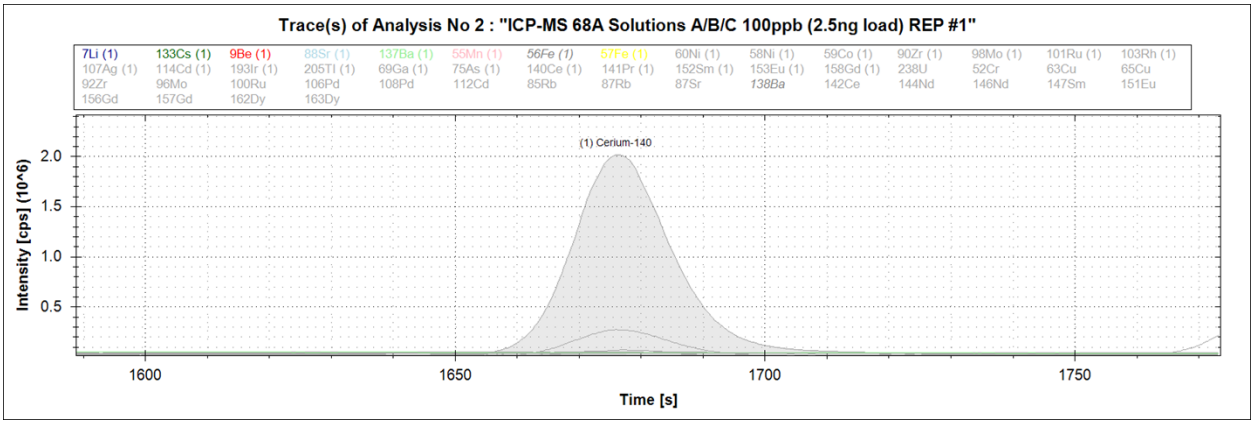

Figure A-20. Elution of cerium, showing a very symmetrical gaussian distribution with no elemental/isobaric overlap.

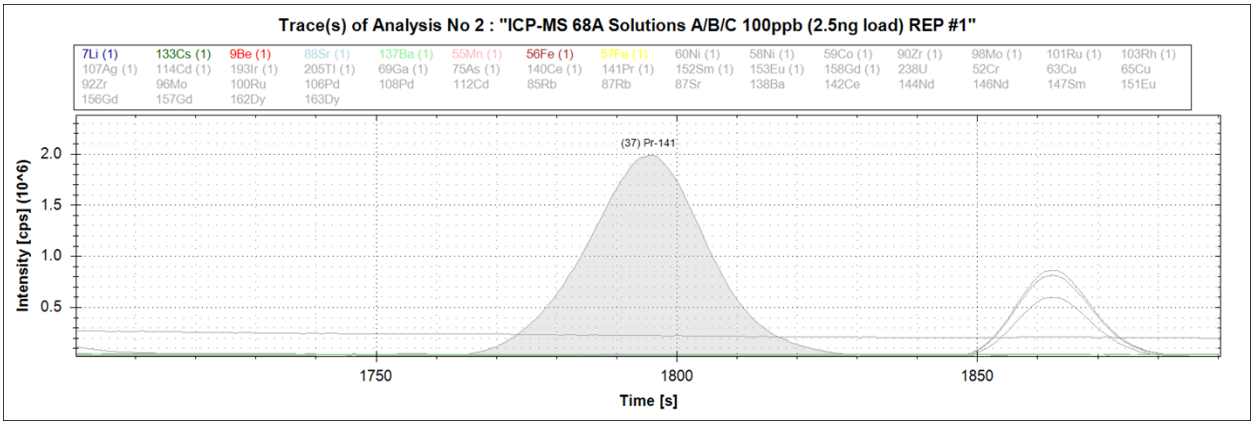

Figure A-21. Elution of praseodymium, showing a very symmetrical gaussian distribution with no elemental overlap.

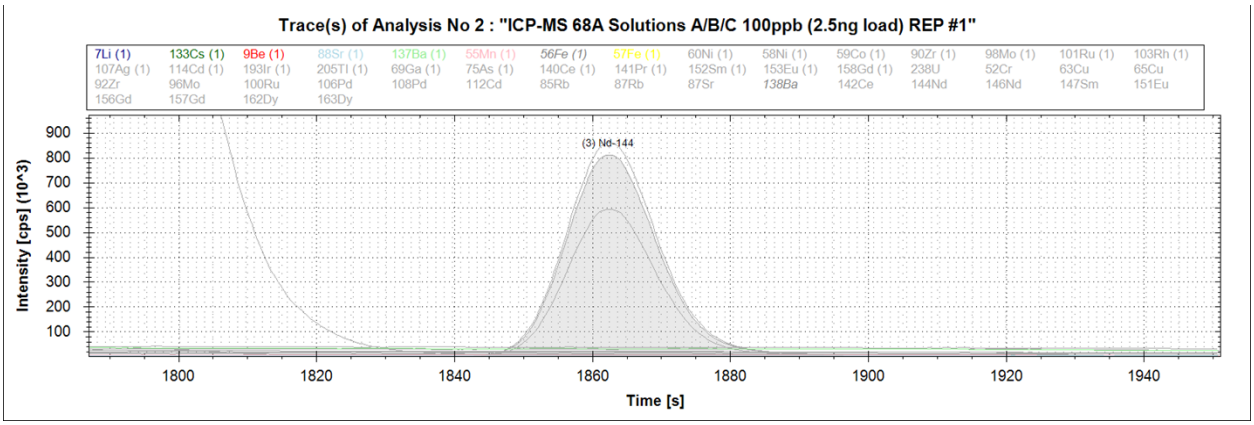

Figure A-22. Elution of neodymium, showing a very symmetrical gaussian distribution with no elemental/isobaric overlap.

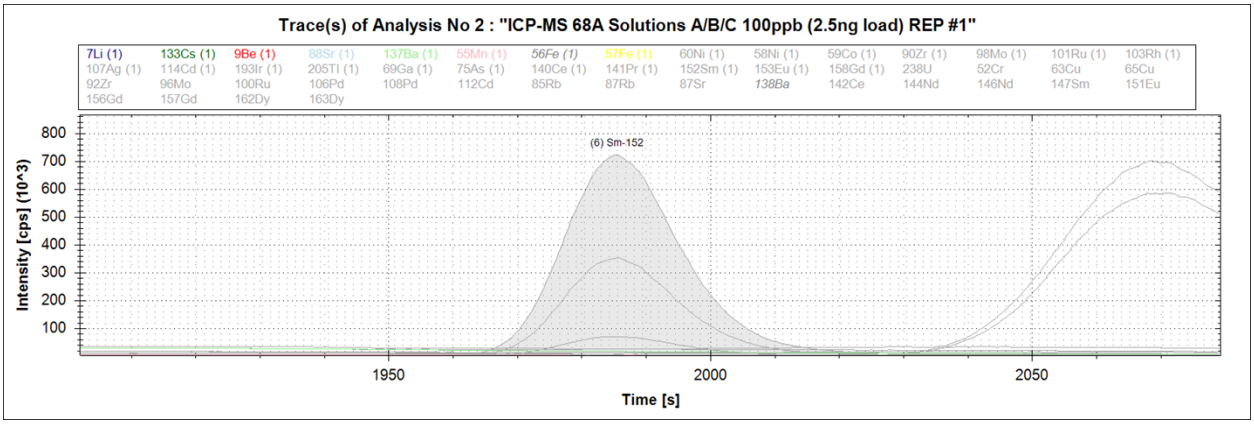

Figure A-23. Elution of samarium, showing a very symmetrical gaussian distribution with no elemental/isobaric overlap.

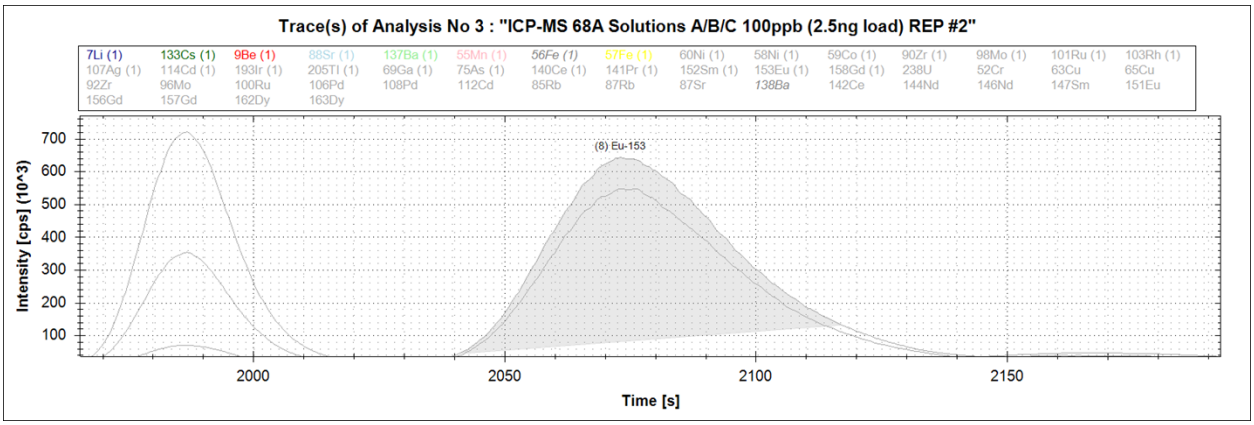

Figure A-24. Elution of europium, showing an elongated distribution with no elemental/isobaric overlap.
Europium may require a different peak picking protocol to increase the allowed baseline window to >50 seconds

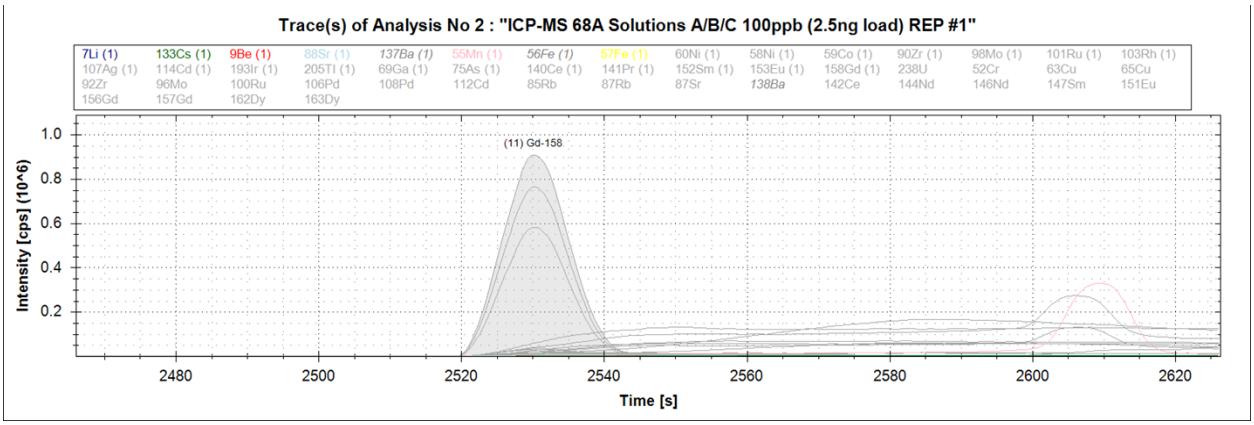

Figure A-25. Elution of samarium, showing a very symmetrical gaussian distribution with no elemental/isobaric overlap.

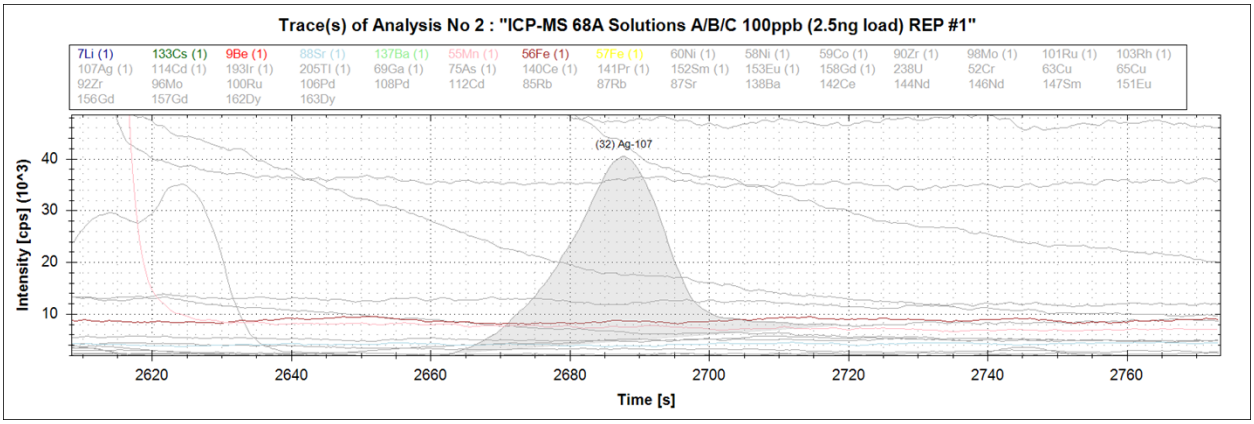

Figure A-26. Elution of silver, with bad symmetry and heavy elemental overlap.
No isobaric overlap shown and elution occurs at two points. Results need to be verified with a concentration study to determine which elution time is more stable.

APPENDIX B. ISOTOPIC CALIBRATION GRAPHS

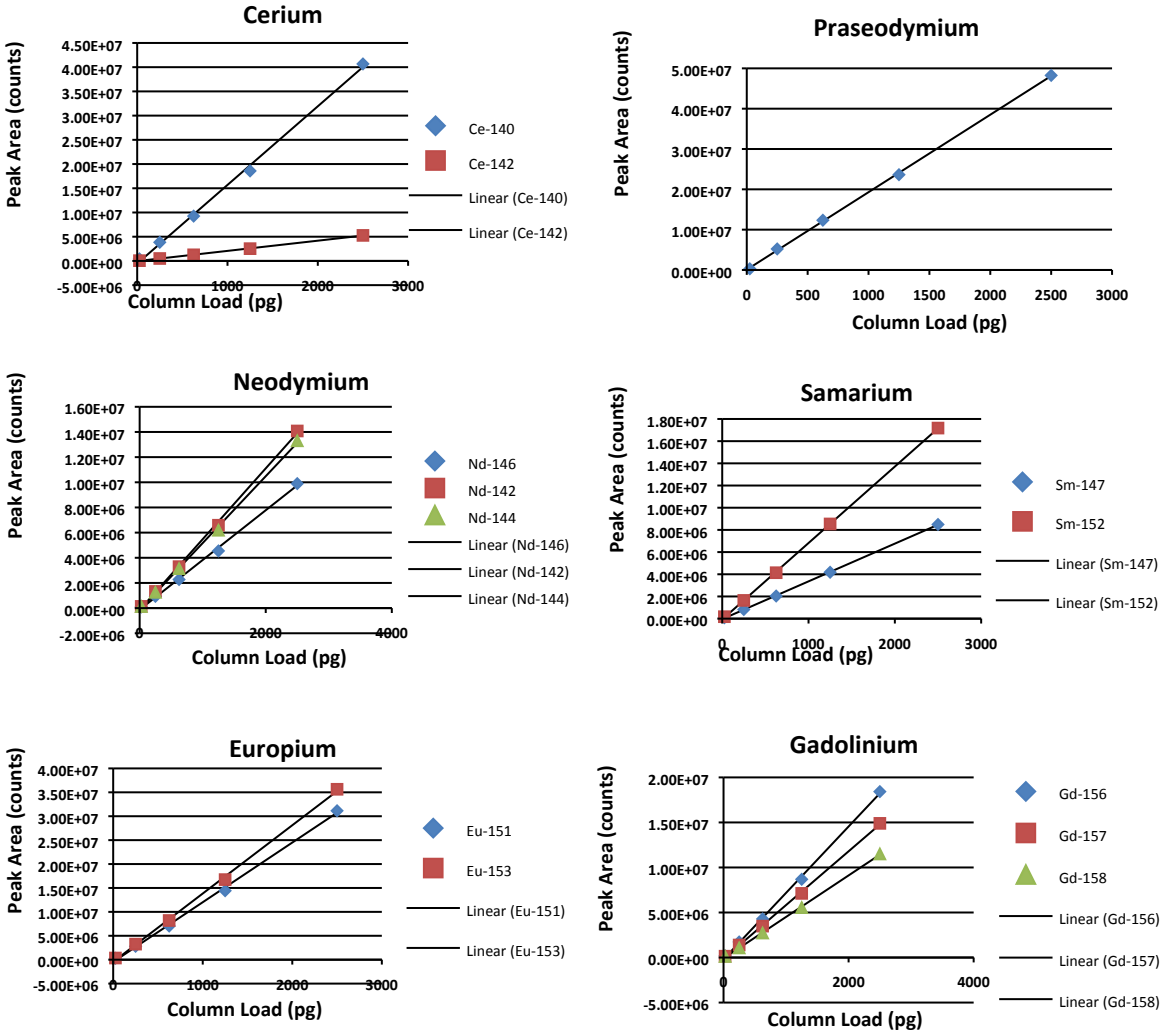

Figure B-1. The calibration graphs for (from top left to bottom right) cerium, praseodymium, neodymium, samarium, europium, and gadolinium. Pictured are the background corrected curves like those that would be used for an external calibration experiment. For the linear regression analysis to determine the limits of detection (LOD) and quantitation (LOQ) values for each isotope, background correction was not applied. The uppermost standard was not included in the calculation because researchers appear to be reaching the upper LOQ at around 2 ng column load.

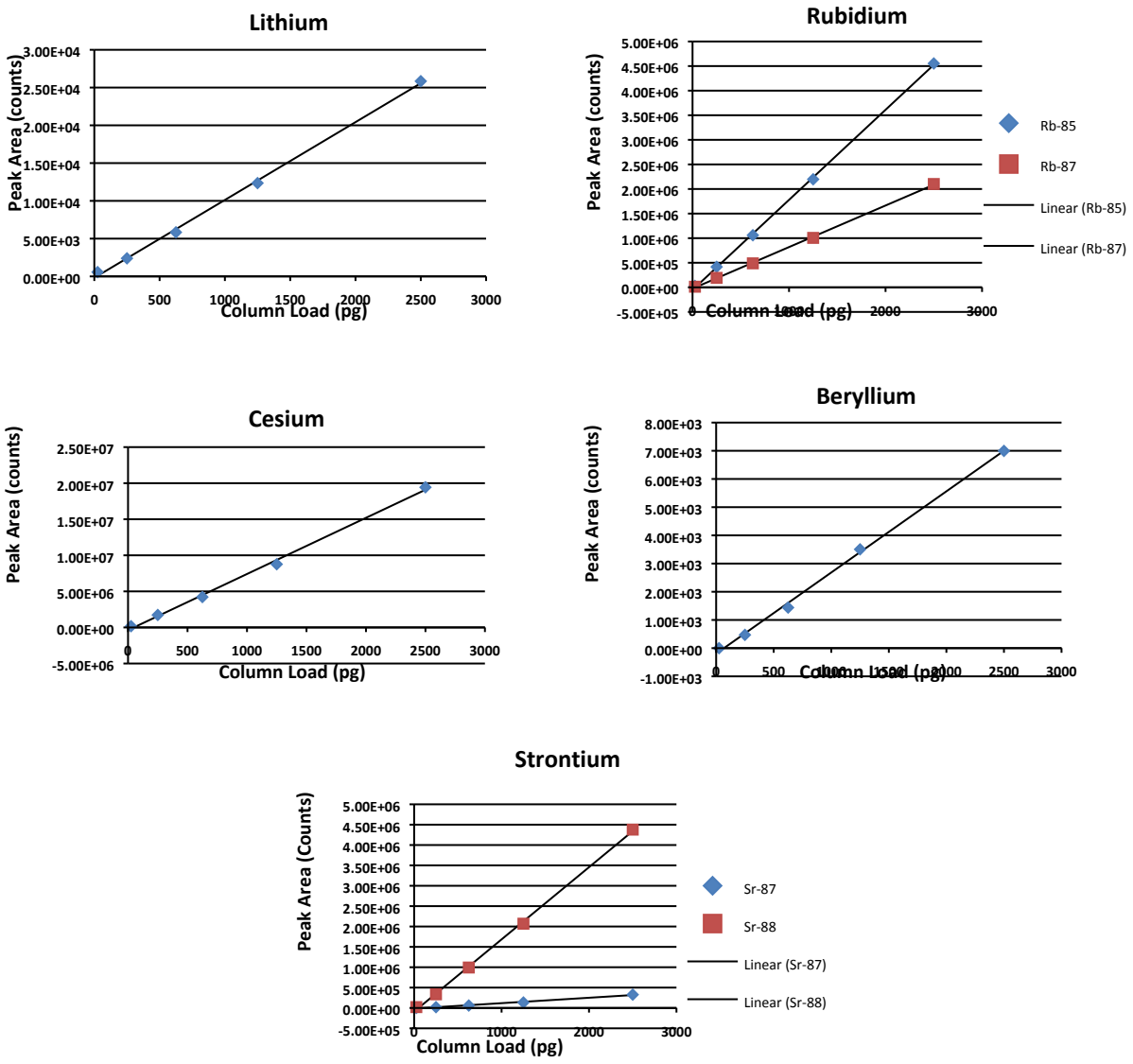

Figure B-2. The calibration graphs for (from top left to bottom center) lithium, rubidium, cesium, beryllium, and strontium. Pictured are the background corrected curves as would be used for an external calibration experiment. For the linear regression analysis to determine the limits of detection (LOD) and quantitation (LOQ) values for each isotope, background correction was not applied. For cesium and rubidium, the uppermost standard was not included in the calculation because researchers appear to be reaching the upper LOQ at around 2 ng column load.

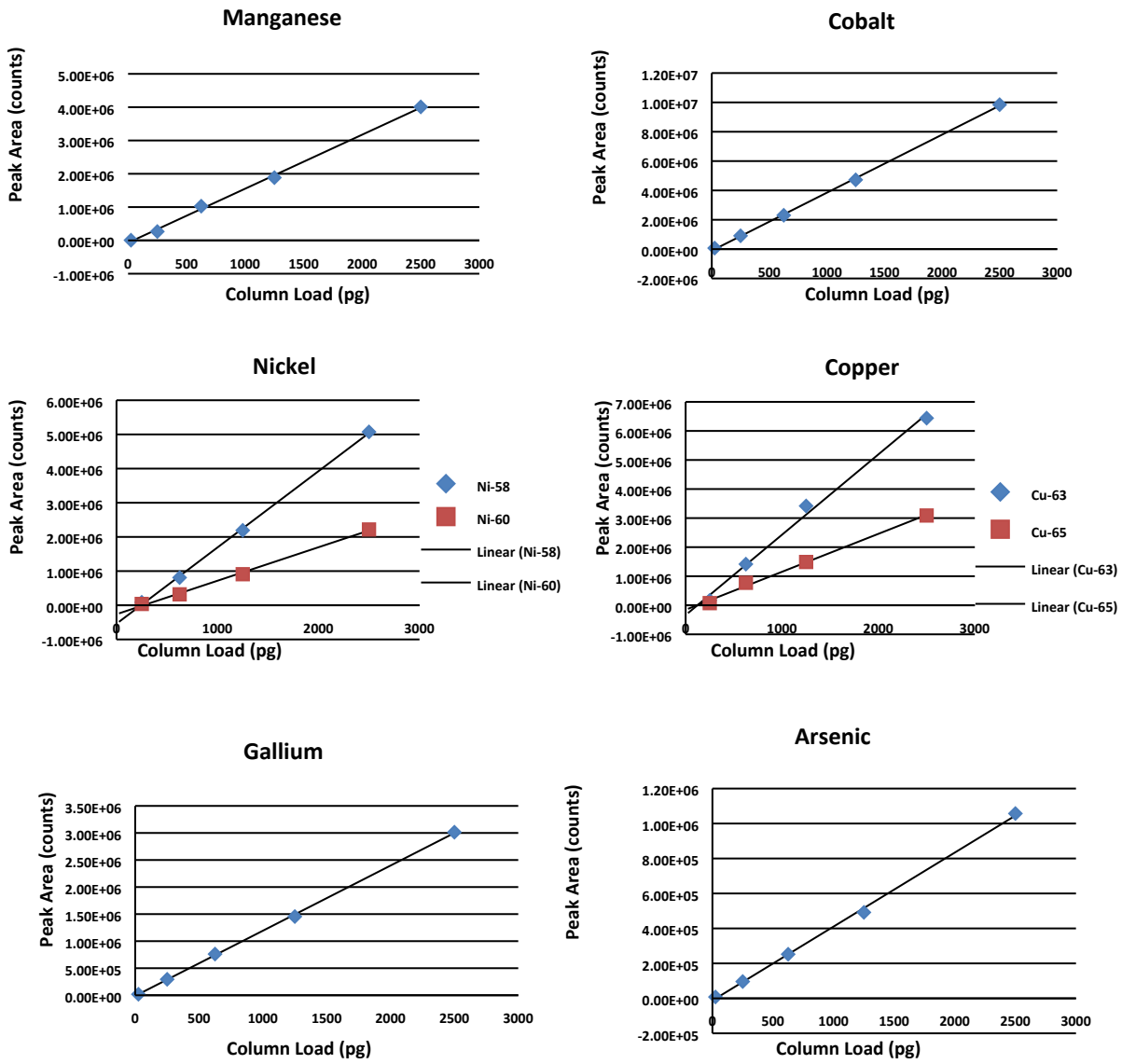

Figure B-3. The calibration graphs for (from top left to bottom right) manganese, cobalt, nickel, copper, gallium, and arsenic. Pictured are the background corrected curves like those that would be used for an external calibration experiment. For the linear regression analysis to determine the limits of detection (LOD) and quantitation (LOQ) values for each isotope, background correction was not applied.

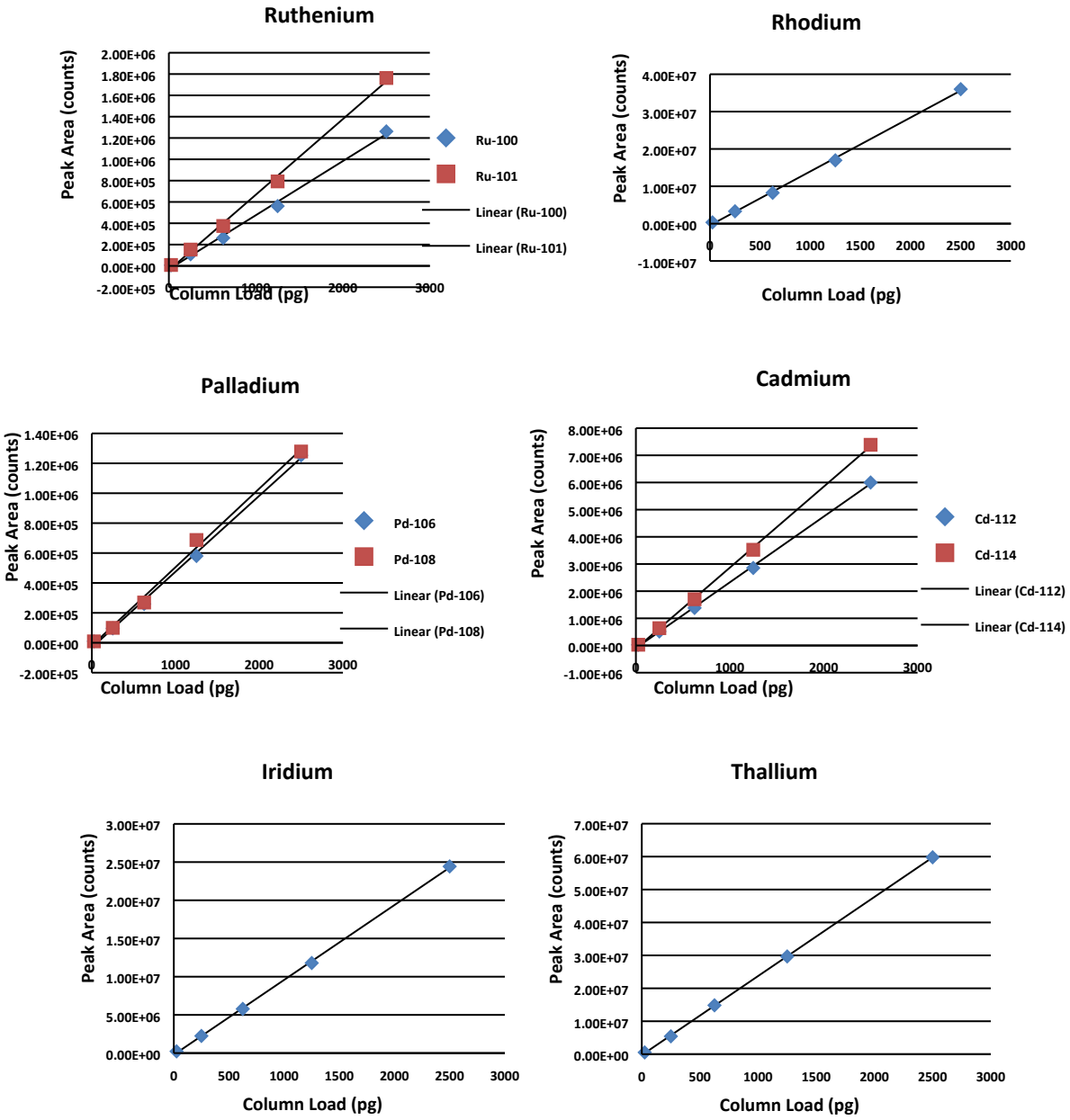

Figure B-4. The calibration graphs for (from top left to bottom right) ruthenium, rhodium, palladium, cadmium, iridium, and thallium. Pictured are the background corrected curves like those that would be used for an external calibration experiment. For the linear regression analysis to determine the limits of detection (LOD) and quantitation (LOQ) values for each isotope, background correction was not applied.